THREE PROBLEMS OF RESONANCE IN COUPLED OR DRIVEN OSCILLATOR SYSTEMS

A Dissertation

Presented to the Faculty of the Graduate School

of Cornell University

in Partial Fulfillment of the Requirements for the Degree of

Doctor of Philosophy

by

Lauren Lazarus

February 2016

THREE PROBLEMS OF RESONANCE IN COUPLED OR DRIVEN OSCILLATOR SYSTEMS

Lauren Lazarus, Ph.D.

Cornell University 2016

The behaviors of three oscillator systems with various types of coupling or driving terms are discussed, with particular regard to their resonance patterns.

In our first problem, a pair of phase-only oscillators are coupled to each other and driven by a third oscillator. By considering the phase differences between each oscillator and the driver, we find the region of parameter space where the system is entrained to the frequency of the driver. A complete analytical equation and multiple approximations for the boundary of this region are discussed. Additionally, the region where the oscillators "drift" relative to the driver is explored by using numerical methods. We find various m:n resonances between the oscillators within this region.

Our second and third problems involve a first-order delay differential equation where the system is found to oscillate provided the delay is greater than a critical value.

In the second problem, two identical delay limit cycle oscillators are coupled via instantaneous linear terms. This system has two invariant manifolds corresponding to in-phase and out-of-phase motions. Behavior on each manifold is expressed as a single delay limit cycle oscillator with an instantaneous self-feedback term. The strength of this self-feedback term changes the critical delay value needed for the system to oscillate. If strong enough, it also creates additional equilibrium solutions and can even prevent the system from oscillating

in a stable way for any amount of delay.

The third problem explores parametric excitation of the delay limit cycle oscillator, by adding a sinusoidal time-varying driving term as a perturbation to the delay value. For most parameter values, this term is non-resonant and causes the system to exhibit quasiperiodic behavior. However, using a two-variable expansion perturbation method, we find a 2:1 resonance between the frequency of the driving term and the natural frequency of the unperturbed oscillator. Expanding about this resonance by a combination of analytical and numerical methods reveals a variety of local and global bifurcations forming the transition between resonant and non-resonant behaviors. The corresponding regions of parameter space are found to hold multiple stable and unstable steady-states.

BIOGRAPHICAL SKETCH

Lauren Lazarus attended the University of New Hampshire and graduated with a Bachelor of Science degree in Physics with University Honors, and a Bachelor of Arts degree in Classics. She began doctoral studies in Theoretical and Applied Mechanics at Cornell University in 2010. At Cornell, Lauren has pursued research in the nonlinear dynamics of oscillator systems under the direction of Professor Richard Rand.

"There is a theory which states that if ever anyone discovers exactly what the Universe is for and why it is here, it will instantly disappear and be replaced by something even more bizarre and inexplicable.
There is another theory which states that this has already happened."
– Douglas Adams, *The Restaurant at the End of the Universe*

ACKNOWLEDGEMENTS

The author wishes to thank her advisor Dr. Richard Rand: for evident ongoing interest in learning and teaching, and the desire to share it with those around him; for his expectations, patience, and hopes; for the community he builds within his group; and for his support and influence on her time at Cornell.

The author also wishes to thank the following:

– Dr. Alexander Vladimirsky, for giving clear and to-the-point advice, and for serving on her committee;
– Dr. Steven Strogatz, for his confidence, and for serving on her committee;
– Matthew Davidow, for his work and involvement in some of this research;
– Shreyas Shah, for interesting discussions about applications to his work;
– Dr. Joseph Tranquillo, for getting her interested and involved in coupled oscillator research as an undergraduate;
– Dr. Maria Terrell, for organizing multiple opportunities to develop her teaching experiences along the way;

And on a more personal note:

– James Melfi, for being her partner and also best friend, for good times and not-so-good times, for knowing each other and facing uncertainty together;
– David Hartino, for being a helpful person and good friend all around, and for giving external perspectives when she needed it most;
– and her family: Joanne and Joseph deKay, Michael and Stephanie Lazarus, et al., for their varying styles of support, clarity, perspectives, and love.

TABLE OF CONTENTS

LIST OF TABLES

LIST OF FIGURES

CHAPTER 1

INTRODUCTION

Limit cycle oscillators have been of great interest to researchers in nonlinear dynamics ever since the time of Rayleigh [1] and van der Pol [2]. There are multiple common models of limit cycle oscillators, including the phase-only oscillator [3] and the van der Pol oscillator.

Additionally, there has been recent interest in oscillator systems with delayed terms. Recent studies have been made of van der Pol oscillators with delayed self–feedback [4], [5] or delayed coupling [6]. It is also possible to model a limit cycle oscillator by a first-order differential equation with a delay term [7]; we consider this model in Chapters 3 and 4.

The upcoming chapters discuss three problems with limit cycle oscillators under some form of coupling or driving. In each system, we identify whether the coupling or driving terms result in resonances and frequency locking, quasiperiodic behavior, or even a lack of oscillation.

We begin in Chapter 2 with a problem of three phase-only oscillators. Some variants of this problem have already been studied [8], [9]. Our focus is on the particular configuration where two of the oscillators are coupled to each other symmetrically and driven by the third oscillator (which might be an external or environmental influence). We use analytical methods to find frequency locking of the full system; we then use numerical methods to find and classify regions of resonance between the coupled pair acting independently from the driver.

In Chapter 3, we introduce a coupled system of two identical delay limit cycle oscillators. The oscillators' in-phase and out-of-phase modes are stud-

ied, wherein the coupled pair acts as a single oscillator with instantaneous self-feedback. Analytical methods and numerical continuation are used to determine regions in parameter space where the system oscillates or settles to a constant steady-state.

Chapter 4 involves a delay limit cycle oscillator which is driven parametrically by a time-varying term in the delay. We use perturbation methods to acquire a non-delayed slow flow system of equations which represents the slowly-varying amplitude of the system's fast oscillation. We then apply analytical and numerical methods to find local and global bifurcations in the slow flow system and identify the stable behaviors of the original oscillator.

For all three systems, we conclude by considering ways that our results may be improved, generalized to other systems, or made more relevant to physical applications.

CHAPTER 2

DYNAMICS OF A SYSTEM OF TWO COUPLED OSCILLATORS DRIVEN BY A THIRD OSCILLATOR

2.1 Abstract

Analytical and numerical methods are applied to a pair of coupled nonidentical phase-only oscillators, where each is driven by the same independent third oscillator. The presence of numerous bifurcation curves defines parameter regions with 2, 4, or 6 solutions corresponding to phase locking. In all cases, only one solution is stable. Elsewhere, phase locking to the driver does not occur, but the average frequencies of the drifting oscillators are in the ratio of m:n. These behaviors are shown analytically to exist in the case of no coupling, and are identified using numerical integration when coupling is included.

2.2 Introduction

Recent experiments in optical laser MEMs have involved models of two coupled oscillators, each of which is being driven by a common harmonic forcer in the form of light [10]. Various steady states have been observed, including complete synchronization, in which both oscillators operate at the same frequency as the forcer, and partial synchronization, in which only one of the oscillators operates at the forcing frequency. Other possible steady states may exist, for example where the two oscillators are mutually synchronized but operate at a different frequency (or related frequencies) than that of the forcer ("relative

locking"). Additionally, the oscillators may operate at frequencies unrelated to each other or to the forcing frequency ("drift"). The question of which of these various steady states is achieved will depend upon both the frequencies of the individual uncoupled oscillators relative to the forcing frequency, as well as upon the nature and strength of the forcing and of the coupling between the two oscillators.

Related studies have been done for other variants of the three coupled oscillator problem. Mendelowitz et al. [8] discussed a case with one-way coupling between the oscillators in a loop; this system resulted in two steady states due to choice of direction around the loop. Baesens et al. [9] studied the general three–oscillator system (all coupling patterns considered), provided the coupling was not too strong, by means of maps of the two–torus.

Cohen et al. [11] modeled segments of neural networks as coupled limit cycle oscillators and discussed the special case of two coupled phase–only oscillators as described by the following:

$$\dot{\theta}_1 = \omega_1 + \alpha \ \sin(\theta_2 - \theta_1) \tag{2.1}$$

$$\dot{\theta}_2 = \omega_2 + \alpha \ \sin(\theta_1 - \theta_2) \tag{2.2}$$

Defining a new variable $\psi = \theta_2 - \theta_1$, being the phase difference between the two oscillators, allows the state of the system to be consolidated into a single equation:

$$\dot{\psi} = \omega_2 - \omega_1 - 2\alpha \ \sin\psi \tag{2.3}$$

This is solved for an equilibrium point (constant ψ) which represents phase locking, i.e. the two oscillators traveling at the same frequency with some constant

separation. This also gives us a constraint on the parameters which allow for phase locking to occur. If no equilibrium point exists, the oscillators will drift relative to each other; while they are affected by each other's phase, the coupling is not strong enough to compensate for the frequency difference.

$$\sin\psi^* = \frac{\omega_2 - \omega_1}{2\alpha} \tag{2.4}$$

$$\left|\frac{\omega_2 - \omega_1}{2\alpha}\right| \leq 1 \tag{2.5}$$

Under the constraint, there are two possible equilibria ψ^* and $(\pi - \psi^*)$ within the domain, though one of them is unstable given that

$$\frac{d\dot{\psi}}{d\psi} = -2\alpha\ \cos(\psi) = -2\alpha(-\cos(\pi - \psi^*))$$

So if one of them is stable ($d\dot{\psi}/d\psi < 0$), the other must be unstable (and vice versa).

Plugging the equilibrium back into the original equations we find the frequency at which the oscillators end up traveling; this is a "compromise" between their respective frequencies.

$$\dot{\theta}_1 = \omega_1 + \alpha\left(\frac{\omega_2 - \omega_1}{2\alpha}\right) = \frac{\omega_1 + \omega_2}{2} \tag{2.6}$$

Since the coupling strength is the same in each direction, the resultant frequency is an average of the two frequencies with equal weight; with different coupling strengths this would become a weighted average.

Keith and Rand [12] added coupling terms of the form $\alpha_2 \sin(\theta_1 - 2\theta_2)$ to this model and correspondingly found 2:1 locking as well as 1:1 locking.

2.3 Model

We design our model, as an extension of the two–oscillator model, to include a pair of coupled phase-only oscillators with a third forcing oscillator, as follows:

$$\dot{\theta}_1 = \omega_1 + \alpha \ \sin(\theta_2 - \theta_1) - \beta \ \sin(\theta_1 - \theta_3) \tag{2.7}$$

$$\dot{\theta}_2 = \omega_2 + \alpha \ \sin(\theta_1 - \theta_2) - \beta \ \sin(\theta_2 - \theta_3) \tag{2.8}$$

$$\dot{\theta}_3 = \omega_3 \tag{2.9}$$

This system can be related back to previous work by careful selection of parameters. Note that the $\beta = 0$ case reduces the system to two coupled oscillators without forcing, while $\alpha = 0$ gives a pair of uncoupled forced oscillators.

It is now useful to shift to a coordinate system based off of the angle of the forcing oscillator, since its frequency is constant. Let $\phi_1 = \theta_1 - \theta_3$ and $\phi_2 = \theta_2 - \theta_3$, with similar relations $\Omega_1 = \omega_1 - \omega_3$ and $\Omega_2 = \omega_2 - \omega_3$ between the frequencies. The forcing oscillator's equation of motion can thus be dropped.

$$\dot{\phi}_1 = \Omega_1 + \alpha \ \sin(\phi_2 - \phi_1) - \beta \ \sin\phi_1 \tag{2.10}$$

$$\dot{\phi}_2 = \Omega_2 + \alpha \ \sin(\phi_1 - \phi_2) - \beta \ \sin\phi_2 \tag{2.11}$$

A nondimensionalization procedure, scaling time with respect to Ω_1, allows for $\Omega_1 = 1$ to be assumed without loss of generality.

We note that the ϕ_i now represent phase *differences* between the paired oscillators and the driver. Thus, if a $\dot{\phi}_i = 0$, the corresponding θ_i is defined to be locked to the driver. Equilibrium points of equations (2.10) and (2.11) then

represent full locking of the system. Partial and total drift are more difficult to recognize and handle analytically, and will be discussed later.

2.4 Full Locking

We begin by solving the differential equations for equilibria directly, so as to find the regions of parameter space for which the system locks to the driver. The equilibria satisfy the equations:

$$0 = 1 + \alpha \ \sin(\phi_2 - \phi_1) - \beta \ \sin\phi_1 \tag{2.12}$$

$$0 = \Omega_2 + \alpha \ \sin(\phi_1 - \phi_2) - \beta \ \sin\phi_2 \tag{2.13}$$

Trigonometrically expanding equation (2.12) and solving for $\cos\ \phi_1$:

$$\cos\ \phi_1 = \frac{\alpha \ \sin\ \phi_1 \ \cos\ \phi_2 + \beta \ \sin\ \phi_1 - 1}{\alpha \ \sin\ \phi_2} \tag{2.14}$$

We square this equation, rearrange it, and use $\sin^2\theta + \cos^2\ \theta = 1$ to replace most cosine terms:

$$\begin{aligned} &\alpha^2\ (1 - \sin^2\ \phi_1)\ \sin^2\ \phi_2 - \alpha^2\ \sin^2\ \phi_1(1 - \sin^2\ \phi_2) \\ &+(2\alpha\ \sin\ \phi_1 - 2\alpha\beta\ \sin^2\ \phi_1)\ \cos\ \phi_2 - \beta^2\ \sin^2\ \phi_1 + 2\beta\ \sin\ \phi_1 - 1 \quad = 0 \end{aligned} \tag{2.15}$$

Repeating the process by solving for $\cos\ \phi_2$, we obtain an equation in terms of only sines:

$$\begin{aligned} -[4\alpha^2\beta^2\ \sin^4\ \phi_1 - 8\alpha^2\beta\ \sin^3\ \phi_1 + (4\alpha^2 - 2\alpha^2\beta^2 - 2\alpha^4)\ \sin^2\ \phi_1 \\ +4\alpha^2\beta\ \sin\ \phi_1 - 2\alpha^2]\ \sin^2\ \phi_2 \\ -\alpha^4\ \sin^4\ \phi_2 - (\beta^4 - 2\alpha^2\beta^2 + \alpha^4)\ \sin^4\ \phi_1 \\ -(4\alpha^2\beta - 4\beta^3)\ \sin^3\ \phi_1 - (6\beta^2 - 2\alpha^2)\ \sin^2\ \phi_1 + 4\beta\ \sin\ \phi_1 - 1 \quad = 0 \end{aligned} \tag{2.16}$$

Returning to equations (2.12) and (2.13), we add them and solve for $\sin\phi_2$ in terms of $\sin\phi_1$:

$$\sin\ \phi_2 = \frac{1+\Omega_2}{\beta} - \sin\ \phi_1 \tag{2.17}$$

This is now plugged into equation (2.16) to eliminate ϕ_2 and obtain an polynomial of degree six in $s = \sin\ \phi_1$, dependent on the various parameters.

$$\begin{aligned}
&-4\alpha^2\beta^6 s^6 + 8\alpha^2\beta^5\Omega_2 s^5 + 16\alpha^2\beta^5 s^5 - 24\alpha^2\beta^4\Omega_2 s^4 - \beta^8 s^4 + 4\alpha^2\beta^6 s^4 \\
&-24\alpha^2\beta^4 s^4 - 4\alpha^2\beta^4\Omega_2^2 s^4 + 8\alpha^2\beta^3\Omega_2^2 s^3 - 4\alpha^2\beta^5\Omega_2 s^3 + 24\alpha^2\beta^3\Omega_2 s^3 \\
&+4\beta^7 s^3 - 12\alpha^2\beta^5 s^3 + 16\alpha^2\beta^3 s^3 + 2\alpha^2\beta^4\Omega_2^2 s^2 - 4\alpha^4\beta^2\Omega_2^2 s^2 \\
&-4\alpha^2\beta^2\Omega_2^2 s^2 + 12\alpha^2\beta^4\Omega_2 s^2 - 8\alpha^4\beta^2\Omega_2 s^2 - 8\alpha^2\beta^2\Omega_2 s^2 - 6\beta^6 s^2 \\
&+14\alpha^2\beta^4 s^2 - 4\alpha^4\beta^2 s^2 - 4\alpha^2\beta^2 s^2 + 4\alpha^4\beta\Omega_2^3 s - 4\alpha^2\beta^3\Omega_2^2 s + 12\alpha^4\beta\Omega_2^2 s \\
&-12\alpha^2\beta^3\Omega_2 s + 12\alpha^4\beta\Omega_2 s + 4\beta^5 s - 8\alpha^2\beta^3 s + 4\alpha^4\beta s - \alpha^4\Omega_2^4 \\
&-4\alpha^4\Omega_2^3 + 2\alpha^2\beta^2\Omega_2^2 - 6\alpha^4\Omega_2^2 + 4\alpha^2\beta^2\Omega_2 - 4\alpha^4\Omega_2 - \beta^4 + 2\alpha^2\beta^2 - \alpha^4 \quad = 0
\end{aligned} \tag{2.18}$$

The roots of this polynomial give values of $s = \sin\ \phi_1$ for a given set of parameter values; degree six implies that there will be up to six roots in s, although a single root in s may correspond to more than one root in ϕ_1 due to the multi-valued nature of sine. To avoid extraneous roots, each should be confirmed in equations (2.12) and (2.13).

In order to distinguish changes in the number of real equilibria, we look for double roots of this polynomial such that two (or more) of the equilibria are coalescing in a single location. Setting the polynomial and its derivative in s equal to zero and using Maxima to eliminate s results in a single equation with 142 terms in α, β, and Ω_2 which describes the location of bifurcations.

$$48\Omega_2^8\alpha^4\beta^4 - 360\Omega_2^8\alpha^6\beta^2 - 32\Omega_2^8\alpha^4\beta^2 - 87\Omega_2^8\alpha^8$$

$$+64\Omega_2^{10}\alpha^6 + 320\Omega_2^9\alpha^6 - 128\Omega_2^7\alpha^4\beta^4 - 1308\Omega_2^7\alpha^6\beta^2$$

$$-112\Omega_2^7\alpha^4\beta^2 - 160\Omega_2^7\alpha^8 + 616\Omega_2^8\alpha^6 + 16\Omega_2^8\alpha^4$$

$$+12\Omega_2^6\alpha^2\beta^8 + 22\Omega_2^6\alpha^4\beta^6 - 16\Omega_2^6\alpha^2\beta^6 + 410\Omega_2^6\alpha^6\beta^4 + 528\Omega_2^7\alpha^6$$

$$+64\Omega_2^7\alpha^4 + 6\Omega_2^6\alpha^4\beta^4 + 8\Omega_2^6\alpha^2\beta^4 + 140\Omega_2^6\alpha^8\beta^2 - 1720\Omega_2^6\alpha^6\beta^2$$

$$-224\Omega_2^6\alpha^4\beta^2 + 256\Omega_2^6\alpha^{10} - 52\Omega_2^5\alpha^2\beta^8 + 324\Omega_2^5\alpha^4\beta^6 + 100\Omega_2^5\alpha^2\beta^6$$

$$+796\Omega_2^6\alpha^8 + 88\Omega_2^6\alpha^6 + 96\Omega_2^6\alpha^4 + 1952\Omega_2^5\alpha^6\beta^4 + 448\Omega_2^5\alpha^4\beta^4$$

$$-48\Omega_2^5\alpha^2\beta^4 - 1240\Omega_2^5\alpha^8\beta^2 - 996\Omega_2^5\alpha^6\beta^2 - 288\Omega_2^5\alpha^4\beta^2 + \Omega_2^4\beta^{12}$$

$$-34\Omega_2^4\alpha^2\beta^{10} + 1536\Omega_2^5\alpha^{10} + 3232\Omega_2^5\alpha^8 - 160\Omega_2^5\alpha^6 + 64\Omega_2^5\alpha^4$$

$$-2\Omega_2^4\beta^{10} - 189\Omega_2^4\alpha^4\beta^8 + 54\Omega_2^4\alpha^2\beta^8 + \Omega_2^4\beta^8 - 480\Omega_2^4\alpha^6\beta^6$$

$$+94\Omega_2^4\alpha^4\beta^6 - 40\Omega_2^4\alpha^2\beta^6 + 960\Omega_2^4\alpha^8\beta^4 + 1526\Omega_2^4\alpha^6\beta^4$$

$$+404\Omega_2^4\alpha^4\beta^4 + 8\Omega_2^4\alpha^2\beta^4 - 1024\Omega_2^4\alpha^{10}\beta^2 - 6284\Omega_2^4\alpha^8\beta^2$$

$$-448\Omega_2^4\alpha^6\beta^2 - 224\Omega_2^4\alpha^4\beta^2 + 3840\Omega_2^4\alpha^{10} + 4726\Omega_2^4\alpha^8 + 88\Omega_2^4\alpha^6$$

$$+108\Omega_2^3\alpha^2\beta^{10} - 152\Omega_2^3\alpha^4\beta^8 - 208\Omega_2^3\alpha^2\beta^8 + 16\Omega_2^4\alpha^4 - 752\Omega_2^3\alpha^4\beta^6$$

$$+100\Omega_2^3\alpha^2\beta^6 + 2560\Omega_2^3\alpha^8\beta^4 + 48\Omega_2^3\alpha^6\beta^6 - 96\Omega_2^3\alpha^6\beta^4$$

$$+448\Omega_2^3\alpha^4\beta^4 - 4096\Omega_2^3\alpha^{10}\beta^2 - 9808\Omega_2^3\alpha^8\beta^2 - 996\Omega_2^3\alpha^6\beta^2$$

$$-112\Omega_2^3\alpha^4\beta^2 + 5120\Omega_2^3\alpha^{10} + 3232\Omega_2^3\alpha^8 + 528\Omega_2^3\alpha^6 - 2\Omega_2^2\beta^{14}$$

$$+30\Omega_2^2\alpha^2\beta^{12} + 68\Omega_2^2\alpha^4\beta^{10} - 56\Omega_2^2\alpha^2\beta^{10} - 2\Omega_2^2\beta^{10} - 320\Omega_2^2\alpha^6\beta^8$$

$$-166\Omega_2^2\alpha^4\beta^8 + 54\Omega_2^2\alpha^2\beta^8 + 512\Omega_2^2\alpha^8\beta^6 + 864\Omega_2^2\alpha^6\beta^6 + 94\Omega_2^2\alpha^4\beta^6$$

$$-16\Omega_2^2\alpha^2\beta^6 + 3200\Omega_2^2\alpha^8\beta^4 + 1526\Omega_2^2\alpha^6\beta^4 + 6\Omega_2^2\alpha^4\beta^4$$

$$-6144\Omega_2^2\alpha^{10}\beta^2 - 6284\Omega_2^2\alpha^8\beta^2 - 1720\Omega_2^2\alpha^6\beta^2 - 56\Omega_2\alpha^2\beta^{12}$$

$$+152\Omega_2\alpha^4\beta^{10} - 32\Omega_2^2\alpha^4\beta^2 + 3840\Omega_2^2\alpha^{10} + 4\Omega_2^2\beta^{12} + 796\Omega_2^2\alpha^8$$

$$+616\Omega_2^2\alpha^6 + 108\Omega_2\alpha^2\beta^{10} - 152\Omega_2\alpha^4\beta^8 - 52\Omega_2\alpha^2\beta^8$$

$$+1024\Omega_2\alpha^8\beta^6 + 48\Omega_2\alpha^6\beta^6 + 324\Omega_2\alpha^4\beta^6 + 2560\Omega_2\alpha^8\beta^4$$

$$+1952\Omega_2\alpha^6\beta^4 - 128\Omega_2\alpha^4\beta^4 - 832\Omega_2\alpha^6\beta^8 - 4096\Omega_2\alpha^{10}\beta^2$$

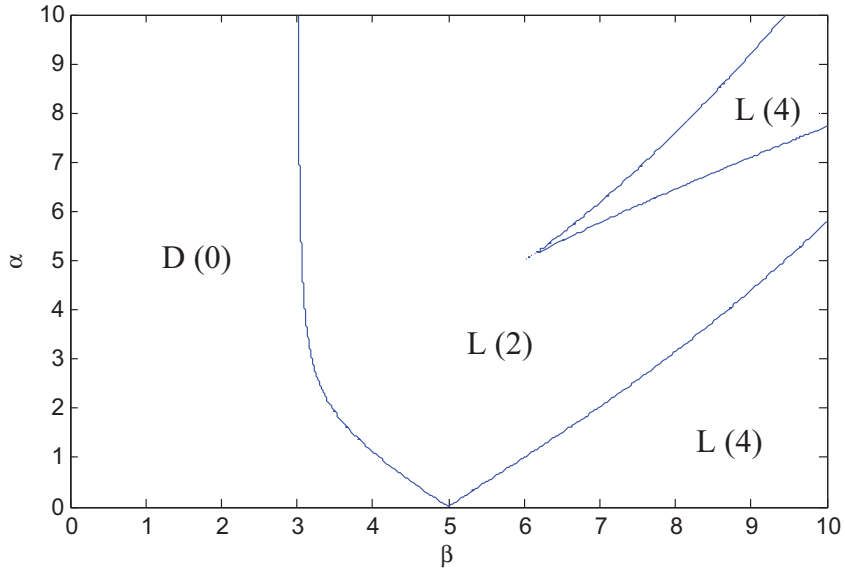

Figure 2.1: $\Omega_2 = 5$ cross-section of surfaces satisfying equation (2.19). Regions show "L" for locking or "D" for drift, followed by number of equilibria.

$$\begin{aligned}
&-1240\Omega_2\alpha^8\beta^2 + \beta^{16} - 12\alpha^2\beta^{14} - 1308\Omega_2\alpha^6\beta^2 + 1536\Omega_2\alpha^{10} \\
&-160\Omega_2\alpha^8 + 320\Omega_2\alpha^6 - 2\beta^{14} + 48\alpha^4\beta^{12} + 30\alpha^2\beta^{12} + \beta^{12} \\
&-64\alpha^6\beta^{10} + 68\alpha^4\beta^{10} - 34\alpha^2\beta^{10} - 320\alpha^6\beta^8 - 189\alpha^4\beta^8 + 12\alpha^2\beta^8 \\
&+512\alpha^8\beta^6 - 480\alpha^6\beta^6 + 22\alpha^4\beta^6 + 960\alpha^8\beta^4 + 410\alpha^6\beta^4 + 48\alpha^4\beta^4 \\
&-1024\alpha^{10}\beta^2 + 140\alpha^8\beta^2 - 360\alpha^6\beta^2 + 256\alpha^{10} - 87\alpha^8 + 64\alpha^6 = 0 \qquad (2.19)
\end{aligned}$$

This equation by itself is cumbersome to work with. We begin to interpret its results by choosing different values of Ω_2 and plotting the resulting curves in the $\beta\alpha$-plane (see Fig. 2.1). Each curve is the location of a double root of the original system, and represents a pair of equilibrium points being created or destroyed in a fold bifurcation. The combination of bifurcation curves leads to regions of 0–6 equilibria.

Numerical analysis of the original differential equations with AUTO contin-

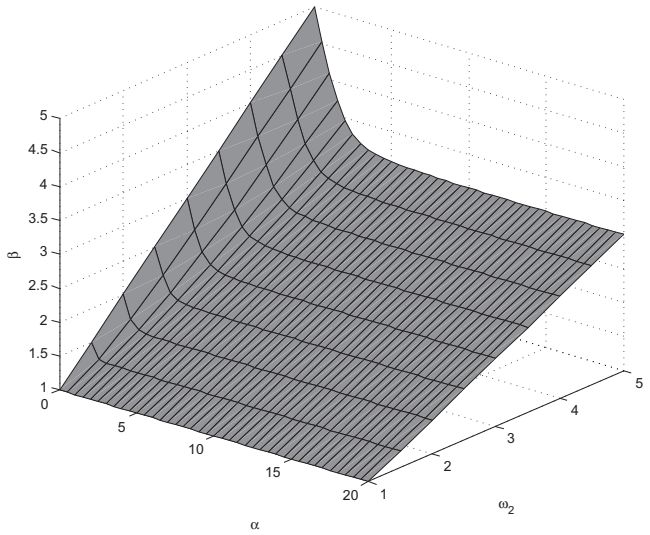

Figure 2.2: Surface of double roots forming the boundary between complete synchronization and the other behaviors.

uation software [13] both confirms the quantities of equilibria and calculates the eigenvalues of each point. Through these results, we find that only one equilibrium point (and therefore locking behavior) is stable; it occurs for any region where equilibria exist, i.e. for large enough forcing strength β.

The leftmost curve, where the first two equilibria are created, is of most interest since it is the boundary between drift and total locking. Figure 2.2 shows only this surface in three dimensions.

2.4.1 Asymptotics

Asymptotic expansions of equation (2.19) may be useful for very large or very small α, in applications where the entire equation would be cumbersome. For these purposes, we assume that $\Omega_2 \geq \Omega_1 = 1$; if this is not true, the two oscillators' labels may be switched such that this analysis is applicable.

Large α Approximation

For large α the curve appears to approach a constant value β. We divide by the highest power, α^{10}, in equation (2.19), then take the limit as α goes to infinity to find that the equation approaches:

$$256\,(\Omega_2+1)^4\,(\Omega_2-2\beta+1)\,(\Omega_2+2\beta+1)=0 \tag{2.20}$$

The middle portion can equal zero for $\Omega_2 \geq 1$, leading to the asymptotic value of β:

$$\beta = \frac{1+\Omega_2}{2} \tag{2.21}$$

We perturb off of this value by writing β as:

$$\beta = \frac{1+\Omega_2}{2} + \frac{k_1}{\alpha} + \frac{k_2}{\alpha^2} + \ldots \tag{2.22}$$

The k_i for odd i are found to be zero, leaving an expression for β with only even terms.

$$\begin{aligned}\beta \;=\; & \frac{1}{2}(\Omega_2+1) + \frac{1}{64\alpha^2}(\Omega_2-1)^2(\Omega_2+1) \\ & + \frac{7}{4096\alpha^4}(\Omega_2-1)^4(\Omega_2+1) \\ & + \frac{(25\Omega_2^2-82\Omega_2+25)}{131072\alpha^6}(\Omega_2-1)^4(\Omega_2+1) + \ldots\end{aligned} \tag{2.23}$$

We note that there is a common factor of $(\Omega_2+1)/2$ present in all terms, which acts as an overall scaling factor for the expression. Figure 2.3 compares this approximation out to 3 and 5 terms in $1/\alpha^2$ with the original numerical result.

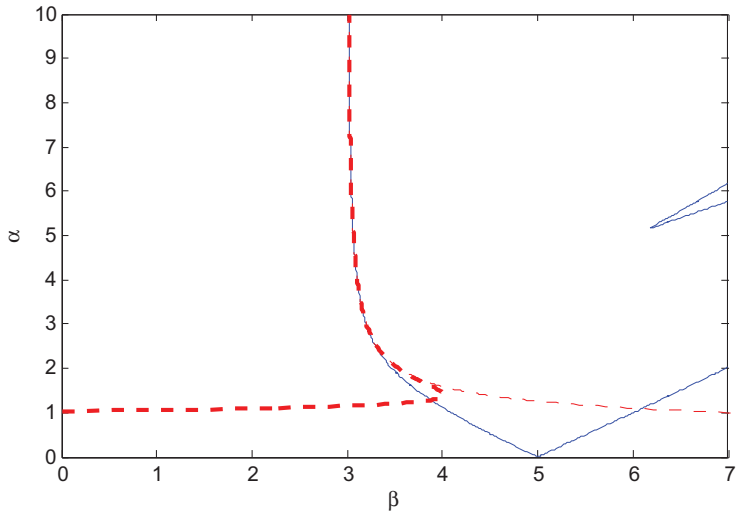

Figure 2.3: Approximations for large α: dashed line accurate to $O(\alpha^{-4})$, bold dashed line to $O(\alpha^{-8})$. $\Omega_2 = 5$.

Small α Approximation

In the $\alpha = 0$ case, the algebraic equations to be solved, eqs. (2.12) and (2.13), become uncoupled:

$$0 = 1 - \beta \sin\phi_1 \tag{2.24}$$

$$0 = \Omega_2 - \beta \sin\phi_2 \tag{2.25}$$

In order for both to have real solutions, $\beta \geq 1$ and $\beta \geq \Omega_2$ must both be satisfied. Thus, under our assumption that $\Omega_2 \geq 1$, equilibria (and therefore locking behavior) will exist for $\beta \geq \Omega_2$.

We perturb off of $\beta = \Omega_2$ for small α in equation (2.19):

$$\beta = \Omega_2 + \mu_1\alpha + \mu_2\alpha^2 + \ldots \tag{2.26}$$

This leads to two different branches, differentiated by the sign of the μ_1 term, due to the intersection of the drift/lock boundary with another bifurcation

curve at $\alpha = 0$. Choosing the drift/lock boundary by taking the negative μ_1 such that β decreases for positive α:

$$\begin{aligned}\beta &= \Omega_2 - \frac{\sqrt{\Omega_2^2 - 1}}{\Omega_2}\alpha + \frac{(2\Omega_2 + 1)}{2\Omega_2^3}\alpha^2 \\ &+ \frac{(\Omega_2^4 + 2\Omega_2^3 - \Omega_2^2 - 2\Omega_2 - 1)}{2\Omega_2^5\sqrt{\Omega_2^2 - 1}}\alpha^3 \\ &+ \frac{(4\Omega_2^6 - 12\Omega_2^4 - 12\Omega_2^3 - \Omega_2^2 + 12\Omega_2 + 5)}{8(\Omega_2 - 1)\Omega_2^7(\Omega_2 + 1)}\alpha^4 \ldots \end{aligned} \tag{2.27}$$

Figure 2.4 shows this approximation out to 5 and 8 terms in α.

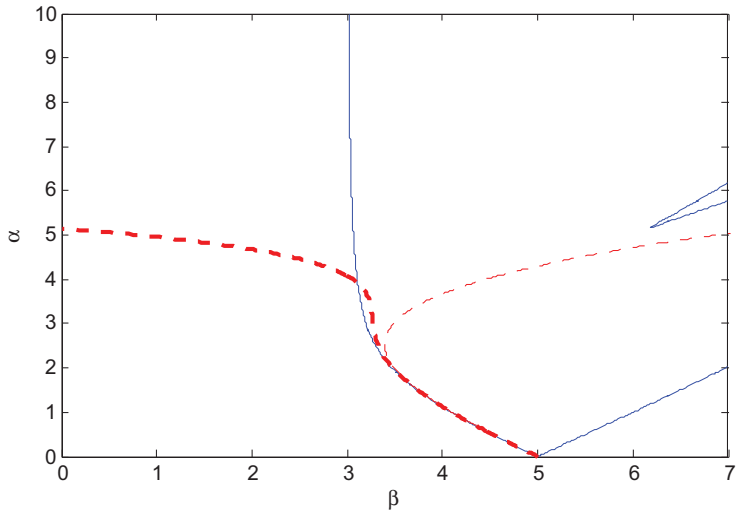

Figure 2.4: Approximations for small α: dashed line accurate to $O(\alpha^4)$, bold dashed line to $O(\alpha^7)$. $\Omega_2 = 5$.

Patched Solution: A Practical Approximation

We approximate the lock/drift boundary curve by two lines for different ranges of α based on their intersection. Our two approximations, taken to be linear:

$$\beta = \frac{1}{2}(\Omega_2 + 1) + O(\alpha^{-2}) \tag{2.28}$$

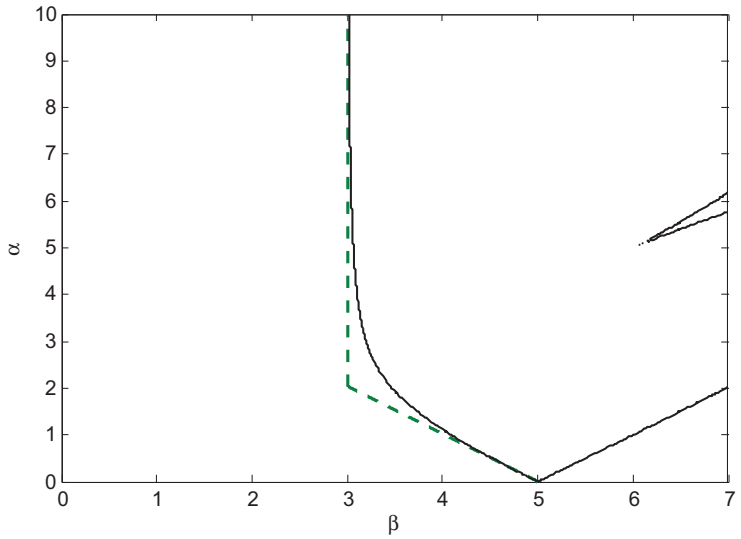

Figure 2.5: Linear piecewise approximation for the drift/lock boundary. $\Omega_2 = 5$.

$$\beta = \Omega_2 - \frac{\sqrt{\Omega_2^2 - 1}}{\Omega_2}\alpha + O(\alpha^2) \tag{2.29}$$

Ignoring nonlinear terms and finding the intersection (β^*, α^*) for a given Ω_2,

$$\beta^* = \Omega_2 - \frac{\sqrt{\Omega_2^2 - 1}}{\Omega_2}\alpha^* = \frac{1}{2}(\Omega_2 + 1) \tag{2.30}$$

$$\alpha^* = \frac{\Omega_2(\Omega_2 - 1)}{2\sqrt{\Omega_2^2 - 1}} = \frac{\sqrt{\beta^* - 1}(2\beta^* - 1)}{2\sqrt{\beta^*}} \tag{2.31}$$

Then we can consider the combined linear approximation to be the piecewise function for β with eq. (2.29) for $\alpha \leq \alpha^*$ and eq. (2.28) for $\alpha \geq \alpha^*$. See Fig. 2.5.

2.5 The Drift Region

Within the region of no equilibrium points, we can study different forms of drift: full drift, m:n relative locking between the ϕ_i while drifting with respect to the driver, or partial synchronization with one oscillator locked to the driver (while the other drifts). To distinguish between these, we start by separately considering the cases $\beta = 0$ and $\alpha = 0$. See Fig. 2.6.

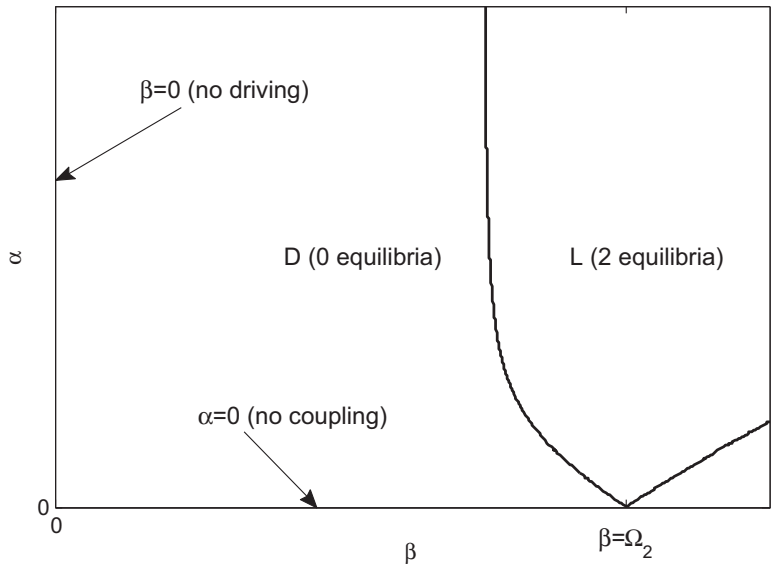

Figure 2.6: Locations of interest for analytical approaches to the drift region.

2.5.1 No Driver $\beta = 0$

We begin with the system with no driver, $\beta = 0$ (as addressed by Cohen et al. [11], see introduction):

$$\dot{\psi} = \frac{d}{dt}(\phi_2 - \phi_1) = \Omega_2 - \Omega_1 - 2\alpha \sin\psi$$

and observe that ϕ_1 and ϕ_2 experience 1:1 phase locking for

$$\alpha \geq |\Omega_2 - 1|/2$$

but there is no locking to θ_3. Thus, corroborating intuition, stronger coupling (larger values of α) results in $1:1$ locking. We would anticipate that this behavior would extend (for nonzero β) into the large$-\alpha$ realm of parameter space, before the driver is strong enough to cause phase locking.

2.5.2 No Coupling $\alpha = 0$

Next, we consider the $\alpha = 0$ case, since the two ϕ_i differential equations become uncoupled and can thus be individually integrated. By separation of variables, we find:

$$dt = \frac{d\phi_1}{1 - \beta \sin \phi_1} = \frac{d\phi_2}{\Omega_2 - \beta \sin \phi_2} \tag{2.32}$$

which can be integrated to find:

$$t(\phi_i) + C_i \quad = \quad 2Q_i \tan^{-1}\left[Q_i\left(\frac{\Omega_i \sin \phi_i}{\cos \phi_i + 1} - \beta\right)\right] \tag{2.33}$$

where

$$Q_i \quad = \quad 1/\sqrt{\Omega_i^2 - \beta^2} \tag{2.34}$$

If we consider a full cycle of ϕ_i, that is, the domain $\phi_0 \leq \phi_i \leq 2\pi + \phi_0$, the argument of the arctangent covers its entire domain of $(-\infty,\ \infty)$ exactly once, so the entire range π of arctangent is covered exactly once. Thus the Δt_i corresponding to this $\Delta\phi_i$ is:

$$\Delta t_i = 2\pi Q_i = 2\pi/\sqrt{\Omega_i^2 - \beta^2} \tag{2.35}$$

Given a known Ω_2 and choosing particular values of β, it should be possible to find a Δt which is an integer multiple of each of the two oscillators' periods. That is, $\Delta t = n_2 \Delta t_1 = n_1 \Delta t_2$ such that in that time, ϕ_1 travels $2\pi n_2$ and ϕ_2 travels $2\pi n_1$. Thus the oscillators would have motion with the ratio $n_1 : n_2$ between their average frequencies.

$$\frac{\Delta t_1}{\Delta t_2} = \frac{n_1}{n_2} = \frac{\sqrt{\Omega_2^2 - \beta^2}}{\sqrt{\Omega_1^2 - \beta^2}} \tag{2.36}$$

By solving for β, we can then pick integers n_i and find the location on $\alpha = 0$ where that type of orbit occurs.

$$\beta^2 = \frac{\Omega_1^2 n_1^2 - \Omega_2^2 n_2^2}{n_1^2 - n_2^2} \tag{2.37}$$

Note that this is not solvable for $n_1 = n_2 = 1$ unless the oscillators are the same and identically influenced by the driver ($\Omega_1 = \Omega_2$); this behavior is instead found on $\beta = 0$ as seen above.

Each ratio $n_1 : n_2$ will have a corresponding β_{n_2/n_1} for $\alpha = 0$; some example values are found in Table 2.1. It is reasonable to think that for small values of α near the β_{n_2/n_1}, the $n_1 : n_2$ behavior might persist although we are no longer able to study the oscillators separately.

2.5.3 Numerical

Based on the $\alpha = 0$ and $\beta = 0$ cases, we expect to find regions of $n_1 : n_2$ relative locking continuing into the rest of the drift region. Through analysis of numerically computed solutions, we focused on cases of $N : 1$ behaviors, though our method should be applicable to more general cases with minor adjustments.

Table 2.1: Example $n_1 : n_2$ locations on $\alpha = 0$ for $\Omega_2 = 1.1$.

n_1	n_2	β_{n_2/n_1}
1	1	does not exist
2	1	0.9644
3	1	0.9868
3	2	0.9121
1	0	$\geq \Omega_1 = 1$

After allowing the system to reach a steady state, we integrate for a $\Delta\phi_1 = 2\pi$ and find the corresponding $\Delta\phi_2$. If this $\Delta\phi_2$ is an integer multiple of 2π, the point in parameter space is classified appropriately as $N : 1$; otherwise, it likely follows some other $n_1 : n_2$ ratio and is not shown. Alternately, if ϕ_1 is constant such that a corresponding $\Delta\phi_2$ would be arbitrary, the point is classified as $1 : 0$ or as an equilibrium.

The results for $0.91 \leq \beta \leq 1.1$, along with the drift/lock boundary curve from above, are shown in Fig. 2.7. (Note that Figs. 2.1-2.5 were calculated for $\Omega_2 = 5$, whereas Figs. 2.7 and 2.8 are for $\Omega_2 = 1.1$.) Some additional tongues were found numerically that also do not appear in the figure, as the higher $N : 1$ tongues are increasingly narrow. We also observe that beyond the edge of Fig. 2.7, the boundary of the $1 : 1$ relative locking region extends to $\alpha = 0.05$ for $\beta = 0$, as expected from our prior calculation.

As anticipated, we find that the tongues of $N : 1$ relative locking emerge from the analytically calculated values on the β axis. These tongues stretch across the $\beta\alpha$-plane and terminate when they reach the drift/lock bifurcation curve.

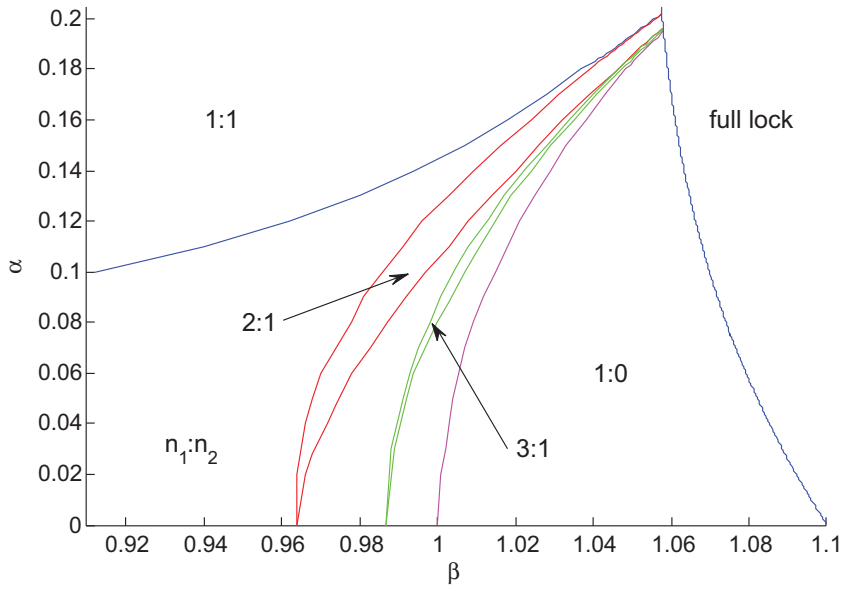

Figure 2.7: $\Omega_2 = 1.1$; numerical $N : 1$ findings and drift/lock bifurcation curve.

Figure 2.8 zooms in on the region of termination; note that the tongues still have nontrivial width when they reach the bifurcation curve.

Figure 2.9 shows a schematic description of the termination of the tongues at the drift/lock bifurcation curve. Each $N : 1$ region disappears in the saddle-node bifurcation in which a pair of equilibria is born (one stable, one unstable), located on the other side of the bifurcation curve. Each $N : 1$ region in the sequence is separated from the next by a region which is filled with other $n_1 : n_2$ tongues.

As N increases, a limit is reached which corresponds to $1 : 0$ locking (i.e. $\infty : 1$). Within this region, ϕ_1 is locked to the driver, but ϕ_2 is not, representing partial synchronization to the driver (rather than relative locking between the oscillators). The curve bounding this region intersects the β axis at $\beta = \Omega_1 = 1$.

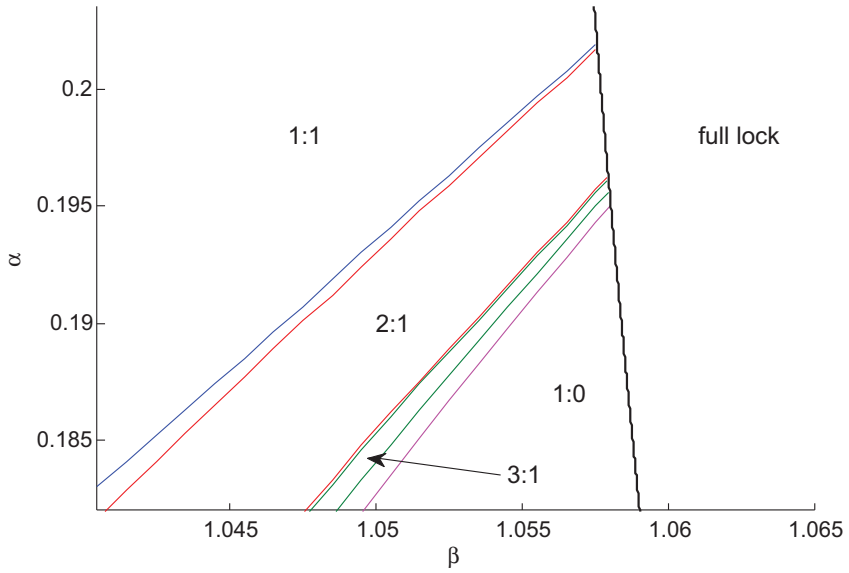

Figure 2.8: Numerical $N:1$ findings and drift/lock boundary zoomed in. $\Omega_2 = 1.1$.

2.6 Conclusion

This work has approached a system of three coupled oscillators which represent a coupled pair under the same periodic external forcing. We investigated the existence of full locking behaviors between the oscillators, and presented two approximations for the boundary between drift and locking based on relative frequencies and coupling strengths. We also studied the various classifications of drift behavior, and their locations in parameter space, including various m:n resonances of the driven pair. In the latter case, the behavior of one oscillator relative to the other is periodic, but the observed behavior of the three-oscillator system is quasiperiodic due to drift relative to the driver.

This project was motivated by the consideration of a pair of coupled oscillators exposed to an environmental forcing. Further work may include the application of this analysis to more realistic models, such as the van der Pol os-

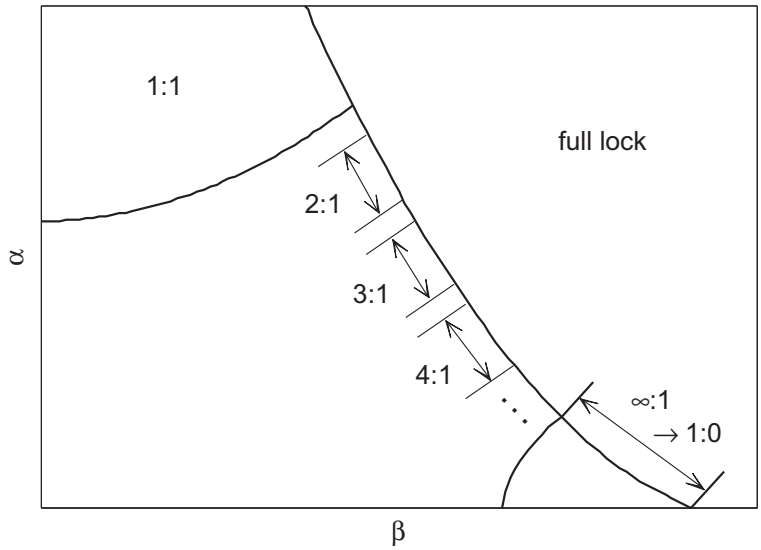

Figure 2.9: Behaviors at the drift/lock boundary curve; not to scale.

cillator, or an expanded set of parameters which could represent nonidentical coupling and driving strengths. Other appropriate considerations would involve the effect of the delay in this problem, or separate environmental drivers, which would both characterize nontrivial distance between the coupled pair of oscillators.

2.7 Acknowledgement

The authors wish to thank Professor Michal Lipson and graduate students Mian Zhang and Shreyas Shah for calling our attention to this problem, which has application to their research.

CHAPTER 3

DYNAMICS OF A DELAY LIMIT CYCLE OSCILLATOR WITH SELF-FEEDBACK

3.1 Abstract

This paper concerns the dynamics of the following nonlinear differential-delay equation:

$$\dot{x} = -x(t-T) - x^3 + \alpha x$$

in which T is the delay and α is a coefficient of self-feedback. Using numerical integration, continuation programs and bifurcation theory, we show that this system exhibits a wide range of dynamical phenomena, including Hopf and pitchfork bifurcations, limit cycle folds and relaxation oscillations.

3.2 Introduction

Coupled oscillators have long been an area of interest in Nonlinear Dynamics. An early effort involved two coupled van der Pol oscillators, [14],[15],[16],[17],[18]. Related work involved coupling two van der Pol oscillators with delayed terms [6].

Besides van der Pol oscillators, other models of coupled limit cycle oscillators have been studied. An important class consists of "phase-only oscillators". These have been studied using algebraic coupling [3],[19],[20],[21],[22] as well as delayed coupling [23].

Recent interest in dynamical systems with delay has produced a new type of oscillator which has the form of a differential-delay equation (DDE):

$$\dot{x} = -x(t - T) - x^3 \tag{3.1}$$

As we shall see, this system exhibits a Hopf bifurcation at $T = \pi/2$ in which a limit cycle is born [24],[25]. We shall refer to eq. (3.1) as a "delay limit cycle oscillator".

The present work is motivated by a study of the dynamics of a system of two coupled delay limit cycle oscillators, each of the form of eq.(3.1):

$$\dot{x} = -x(t - T) - x^3 + \alpha y \tag{3.2}$$

$$\dot{y} = -y(t - T) - y^3 + \alpha x \tag{3.3}$$

In particular we focus on the dynamics on the in-phase mode, $x = y$. Flow on this invariant manifold satisfies the DDE:

$$\dot{x} = -x(t - T) - x^3 + \alpha x \tag{3.4}$$

Eq. (3.4), which may be described as a delay limit cycle oscillator with self–feedback, is the subject of this paper.

3.3 Equilibria and their Stability

Equilibria in eq. (3.4) are given by the equation

$$0 = -x - x^3 + \alpha x \tag{3.5}$$

For $\alpha < 1$, only $x = 0$ is a solution. For $\alpha \geq 1$, an additional pair of solutions $x = \pm\sqrt{\alpha - 1}$ exist such that there are 3 constant solutions. These solutions emerge from the $x = 0$ solution in a pitchfork bifurcation at $\alpha = 1$.

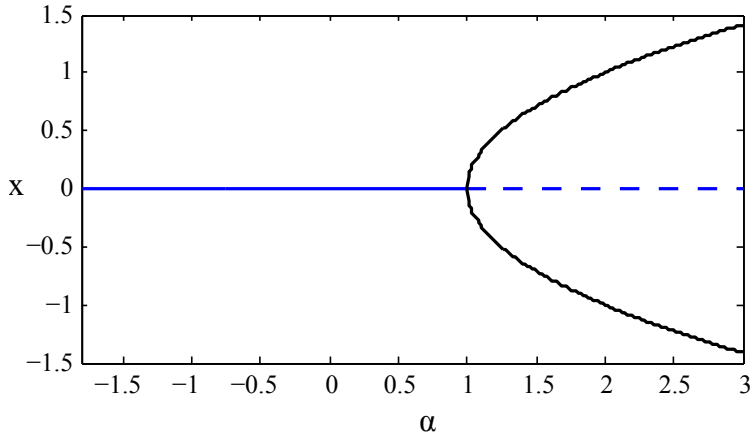

Figure 3.1: Locations of equilibria as a function of α, independent of T.

In order to determine the stability of the equilibrium at $x = 0$, we investigate the linearized DDE:

$$\dot{x} = -x(t - T) + \alpha x \tag{3.6}$$

Setting $x = Ae^{\lambda t}$, we obtain the characteristic equation:

$$\lambda = -e^{-\lambda T} + \alpha \tag{3.7}$$

In the zero–delay ($T = 0$) case, we are left with $\lambda = \alpha - 1$; therefore $x = 0$ is stable for $\alpha < 1$ and becomes unstable for $\alpha > 1$ where the other equilibria (the arms of the pitchfork) exist.

For non–zero delay ($T > 0$), we anticipate the existence of a Hopf bifurcation and the creation of a limit cycle, based on the known behavior for $\alpha = 0$. We

look for pure imaginary eigenvalues by substituting $\lambda = i\omega$ into the characteristic equation (3.7) and separating the real and imaginary terms into separate equations:

$$\omega = \sin(\omega T) \tag{3.8}$$

$$0 = -\cos(\omega T) + \alpha \tag{3.9}$$

By manipulating these we obtain:

$$\sin^2(\omega T) + \cos^2(\omega T) = \omega^2 + \alpha^2 = 1 \tag{3.10}$$

$$T_H = \frac{\arccos \alpha}{\omega} = \frac{\arccos \alpha}{\sqrt{1-\alpha^2}} \tag{3.11}$$

So for a given α, there exists a delay T_H where a Hopf bifurcation occurs at $x = 0$. In this case, the Hopf bifurcations only exist for $-1 < \alpha < 1$, since real ω and finite T_H cannot exist otherwise. Note that for $\alpha = 0$ (which corresponds to the uncoupled oscillator of eq. (3.1)), the Hopf occurs at $T_H = \pi/2$. Fig. 3.2 shows the stability of the $x = 0$ equilibrium point in α-T space.

Next we consider the stability of the equilibria located along the arms of the pitchfork at

$$x = \pm\sqrt{\alpha - 1} \tag{3.12}$$

We begin by setting $x = \pm\sqrt{\alpha - 1} + z$ which gives the following nonlinear DDE:

$$\dot{z} = -z(t-T) + (3-2\alpha)z \mp 3\sqrt{\alpha-1}z^2 - z^3 \tag{3.13}$$

Stability is determined by linearizing this equation about $z = 0$:

$$\dot{z} = -z(t-T) + (3-2\alpha)z \tag{3.14}$$

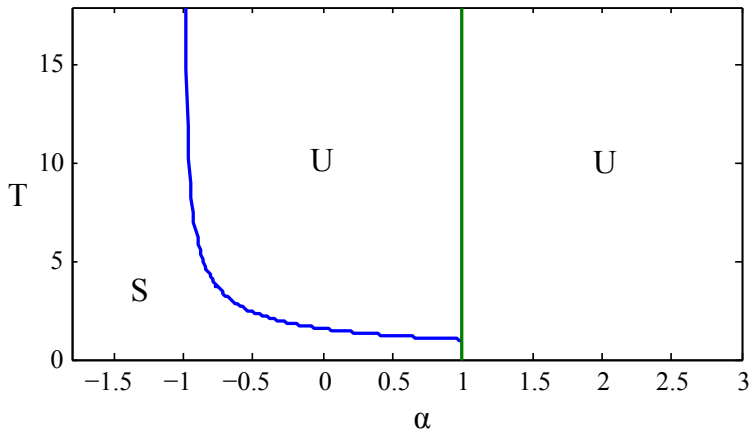

Figure 3.2: Stability diagram for the equilibrium at $x = 0$. Regions are marked for the equilibria being stable (S) or unstable (U). The curved line is given by the Hopf eq. (3.11). The instability for $\alpha > 1$ is due to a pitchfork bifurcation.

Note that this is the same as eq. (3.6) with α replaced by $(3 - 2\alpha)$. Thus we use eq. (3.11) to find the critical delay for Hopf bifurcation as:

$$T_H = \frac{\arccos(3 - 2\alpha)}{\sqrt{1 - (3 - 2\alpha)^2}} \tag{3.15}$$

Fig. 3.3 shows the existence and stability of the equilibria located at $x = \pm\sqrt{\alpha - 1}$.

3.4 Limit Cycles

We have seen in the foregoing that eq. (3.4) exhibits various Hopf bifurcations, each generically yielding a limit cycle. We are concerned about the following questions regarding these limit cycles:

(a) are they stable, i.e., are the Hopf bifurcations supercritical?

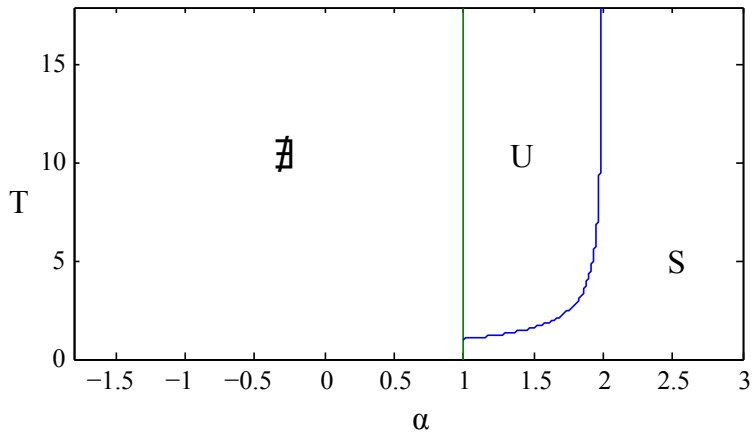

Figure 3.3: Stability diagram for the equilibria at $x = \pm\sqrt{\alpha - 1}$. Regions are marked for the equilibria being nonexistent, unstable or stable. The curved line is given by the Hopf eq. (3.15).

(b) what happens to the limit cycles after they are born in the Hopfs?

The question of the stability of the limit cycles may be answered by applying the multiple scales perturbation method to the nonlinear DDEs (3.4) and (3.13). In fact this has already been accomplished in [26] for a general DDE of the form:

$$\frac{du}{dt} = \gamma u + \beta u_d + a_1 u^2 + a_2 u u_d + a_3 u_d^2 + b_1 u^3 + b_2 u^2 u_d + b_3 u u_d^2 + b_4 u_d^3 \tag{3.16}$$

where $u = u(t)$ and $u_d = u(t - T)$. The results of that reference are given in the Appendix. When applied to eq. (3.4), we find that the amplitude A of the limit cycle is given by the expression:

$$A^2 = \frac{-4(\alpha^2 - 1)^2}{3(\alpha\sqrt{1 - \alpha^2}\arccos\alpha + \alpha^2 - 1)}\,\mu \tag{3.17}$$

where μ is the detuning off of the critical delay,

$$T = T_H + \mu, \tag{3.18}$$

and where the approximate form of the limit cycle is $x = A\cos\omega t$. Here T_H and ω are given by eqs. (3.10) and (3.11). A plot of the coefficient of μ in eq. (3.17) is

given in Fig. 3.4 for $-1 < \alpha < 1$. Note that this coefficient is non-negative over this parameter range (cf. Fig. 3.2), which means that the limit cycle occurs for positive μ, i.e. for $T > T_H$, i.e. when the equilibrium at $x = 0$ is unstable. Since the Hopf occurs in a 2-dimensional center manifold, this shows that the Hopf is supercritical and the limit cycle is stable.

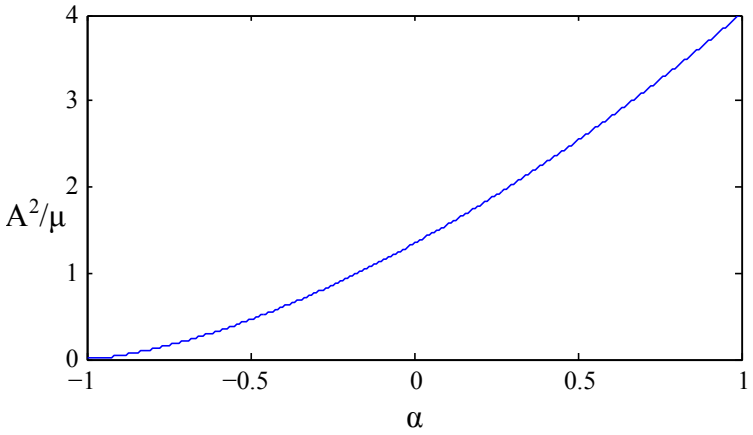

Figure 3.4: The coefficient of μ in eq. (3.17) is plotted for $-1 < \alpha < 1$. Its non-negative value shows that the limit cycle is stable, see text.

A similar analysis may be performed for limit cycles born from equilibria located on the arms of the pitchfork bifurcation. In this case we use eq. (3.13) and find that the limit cycle is unstable, and that the Hopf is subcritical.

These results have been confirmed by comparison with numerical integration of eq. (3.4) using the MATLAB function DDE23 and the continuation software DDE-BIFTOOL [27], [28], [29]. Fig. 3.5 shows a limit cycle obtained by using DDE23 for delay T=4 and α=−0.75. For these parameters, eq. (3.11) gives T_H=3.6570 and eq. (3.17) gives a limit cycle amplitude of A=0.2312. Also, eq.

(3.10) gives ω=0.6614, which gives a period of $2\pi/\omega$=9.4993. Note that these computed values agree with the values obtained by numerical simulation in Fig. 3.5.

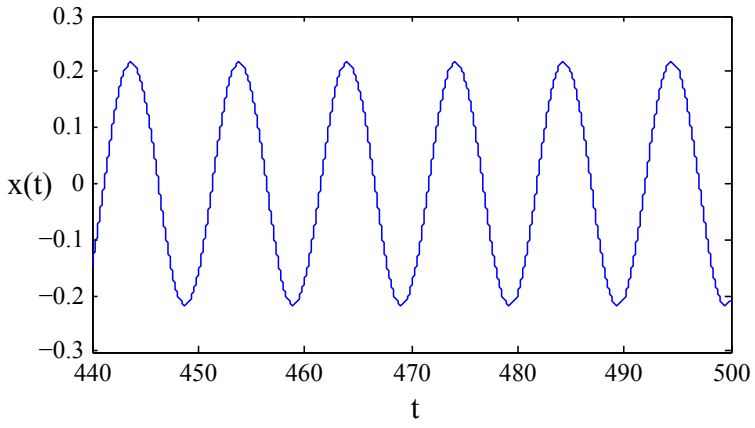

Figure 3.5: Limit cycle obtained by using DDE23 for delay T=4 and α=−0.75. The theoretical values of amplitude and period, namely A=0.2312 and period=0.6614 (see text) agree well with those seen in the simulation.

The DDE-BIFTOOL software shows that the limit cycles born in a Hopf from the equilibrium at $x = 0$, die in a limit cycle fold. Fig. 3.6 displays two DDE-BIFTOOL plots of limit cycle amplitude ($\times$ 2) versus α for $T = 1.1$ and $T = 3.5$. The collection of all such curves is a surface in α-T-Amplitude space and is displayed in Fig. 3.7. Note that although the locus of limit cycle fold points cannot be found analytically, an approximation for it may be obtained from the DDE-BIFTOOL curves and is shown in Fig. 3.7. When projected down onto the α-T plane, it represents the boundary beyond which there are no stable limit cycles.

As noted above, the Hopf bifurcations off of the equilibria located on the arms of the pitchfork are subcritical, i.e. the resulting limit cycle is unstable. This is illustrated in Fig. 3.8 which is a DDE-BIFTOOL computation showing

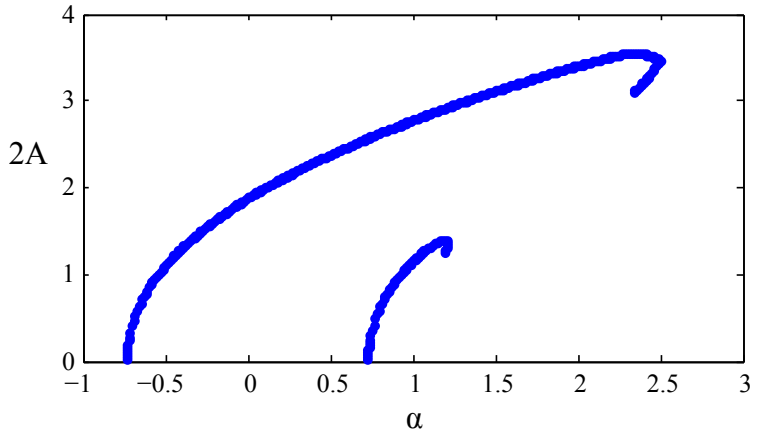

Figure 3.6: DDE-BIFTOOL plots of limit cycle amplitude (x 2) versus α. The smaller curve is for $T = 1.1$ and the larger one is for $T = 3.5$. Note that the limit cycles are born in a Hopf bifurcation and die in a limit cycle fold, i.e. by merging with an unstable limit cycle in a saddle-node bifurcation of cycles.

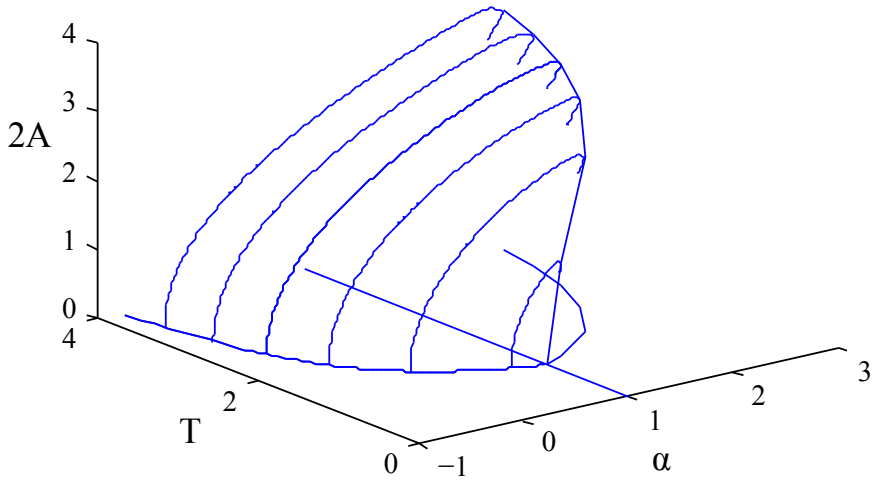

Figure 3.7: A surface of limit cycles. Each limit cycle is born in a Hopf and dies in a limit cycle fold. The locus of limit cycle fold points is shown as a space curve, and is also shown projected down onto the α-T plane.

the Hopf bifurcation at $\alpha = 1.5$ for varying delay T. Eq. (3.15) gives the critical value $T_H = \pi/2$.

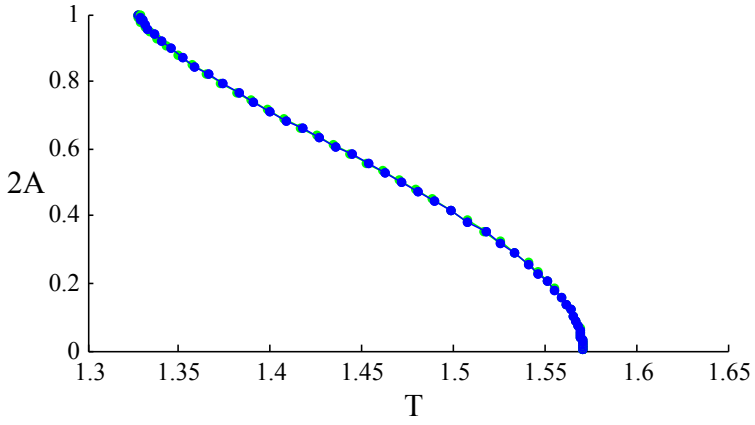

Figure 3.8: DDE-BIFTOOL plot showing Hopf off of the equilibrium at $x = \sqrt{\alpha - 1} = 0.7071$ for $\alpha = 1.5$, for varying delay T. Note that eq. (3.15) gives the critical value $T_H = \pi/2$.

3.5 Large Delay

Numerical simulation of eq. (3.4) shows that for large values of delay, the limit cycles take the form of a an approximate square wave, see Fig. 3.9. The following features have been observed in numerical simulations (cf. Fig. 3.9):

1. The period of the square wave is approximately equal to twice the delay, $2T$.
2. The amplitude of the square wave is approximately equal to $\sqrt{1 + \alpha}$.
3. The large delay square wave is not found in simulations for which α >3.

In this section we offer analytic explanations for these observations.

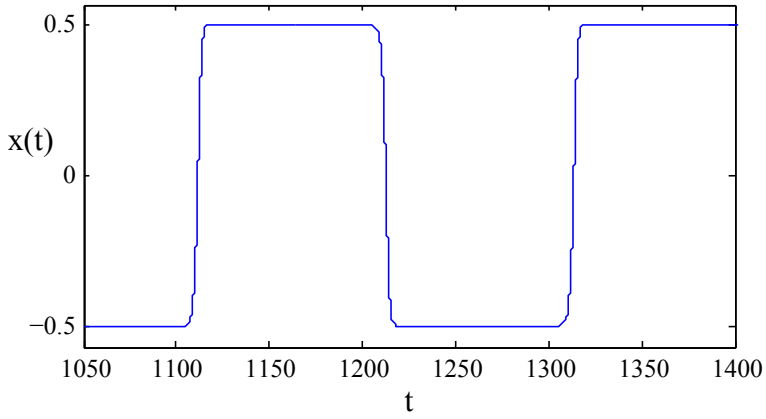

Figure 3.9: Limit cycle obtained by using DDE23 for delay T=100 and α=−0.75. Note the approximate form of a square wave, in contrast to the nearly sinsusoidal wave shape for smaller values of delay, cf. Fig. 3.5.

Since eq. (3.4) is invariant under the transformation $x \mapsto -x$, we may refer to the value at the upper edge of the square wave as $x = A > 0$, in which case the value at the lower edge is $x = -A$. Then at a point $x(t)$ on the lower edge, $x(t-T)$ refers to a point on the upper edge, $x(t-T) = A$, and eq. (3.4) becomes:

$$0 = -A - (-A)^3 + \alpha(-A) \tag{3.19}$$

which gives the nontrivial solution

$$A = \sqrt{\alpha + 1} \tag{3.20}$$

Note that if $\alpha < -1$, this solution cannot exist, no matter what the delay T is.

During a jump down, $x(t-T)$ again takes on the value $\sqrt{\alpha+1}$, so that (3.4) becomes

$$\frac{dx}{dt} = -\sqrt{\alpha+1} - x^3 + \alpha x \tag{3.21}$$

Eq. (3.21) has equilibria at

$$x = -\sqrt{\alpha+1},\ x = \frac{\sqrt{\alpha+1} \pm \sqrt{\alpha-3}}{2} \tag{3.22}$$

For $\alpha < 3$ there is only one real root, $x = -A = -\sqrt{\alpha + 1}$.

During the jump down, the variable x starts at $\sqrt{\alpha + 1}$, which acts like an initial condition for the jump according to eq. (3.21). The motion continues in x towards the equilibrium at $x = -\sqrt{\alpha + 1}$, which is approached for large time t. Note that the other two equilibria in eq. (3.22) lie between $x = -\sqrt{\alpha + 1}$ and $x = \sqrt{\alpha + 1}$ in the case that $\alpha > 3$. Their presence prevents x from approaching $x = -\sqrt{\alpha + 1}$ and thus disrupts the jump, which explains why no square wave limit cycles are observed for $\alpha > 3$.

The foregoing argument assumes that the equilibrium at $x = -\sqrt{\alpha + 1}$ is stable. To investigate the stability of the equilibrium at $x = -\sqrt{\alpha + 1}$, we set

$$x = -\sqrt{\alpha + 1} + y \tag{3.23}$$

Substituting (3.23) into (3.21), we obtain

$$\frac{dy}{dt} = -y^3 + 3\sqrt{\alpha + 1}y^2 - (2\alpha + 3)y \tag{3.24}$$

Linearizing (3.24) for small y shows that $x = -\sqrt{\alpha + 1}$ is stable for $\alpha > -3/2$. Since the square wave solution ceases to exist when $\alpha < -1$, the restriction of $\alpha > -3/2$ is not relevant.

3.6 Discussion

In the foregoing sections we have shown that the delay limit cycle oscillator with self-feedback, eq. (3.4), supports a variety of dynamical phenomena, in-

cluding Hopf and pitchfork bifurcations, limit cycle folds and relaxation oscillations. Numerical explorations using DDE-BIFTOOL have revealed that eq. (3.4) exhibits many additional bifurcations, see e.g. Fig. 3.10.

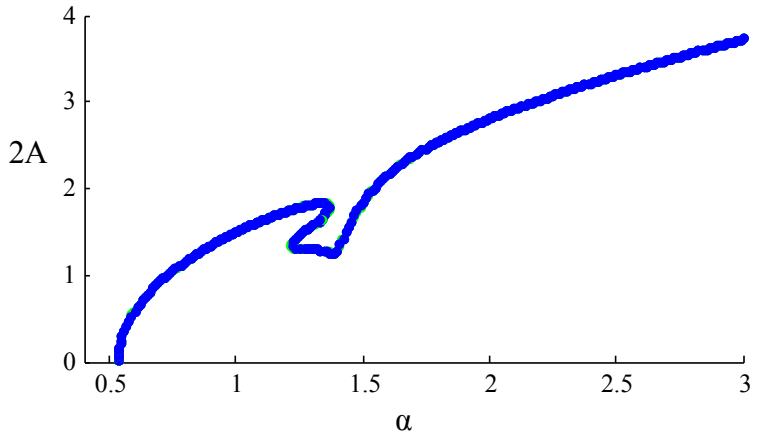

Figure 3.10: Numerical simulation of eq. (3.4) for $T = 1.19$ using DDE-BIFTOOL. Note that the left portion of the continuation curve is similar to those shown in Figs. 3.6 and 3.7. However the additional bifurcations shown have not been identified. The periodic motions represented by the rest of the branch could not be found using DDE23 and are evidently unstable.

We also note that due to the multivalued nature of arccosine, there are an infinite number of Hopf bifurcation curves in parameter space. Referring to eqs. (3.11) and (3.15), these Hopf bifurcation curves can be generalized to:

$$T_H = \frac{(2\pi n + \arccos \alpha)}{\sqrt{1-\alpha^2}} \tag{3.25}$$

$$T_H = \frac{(2\pi n + \arccos(3-2\alpha))}{\sqrt{1-(3-2\alpha)^2}} \tag{3.26}$$

for integer n, where the $n = 0$ case represents the bifurcations already discussed. We use the principal value of arccosine in this definition to be consistent with the original equations.

These additional bifurcations do not change the overall stability of the equi-

libria. The related periodic motions appear to be unstable and have not been observed in the results of DDE23 simulation. We can use numerical continuation in DDE-BIFTOOL to trace them for varying delay T; for instance, Fig. 3.11 shows results for the motions created by the $n = 0$ and $n = 1$ Hopf bifurcations.

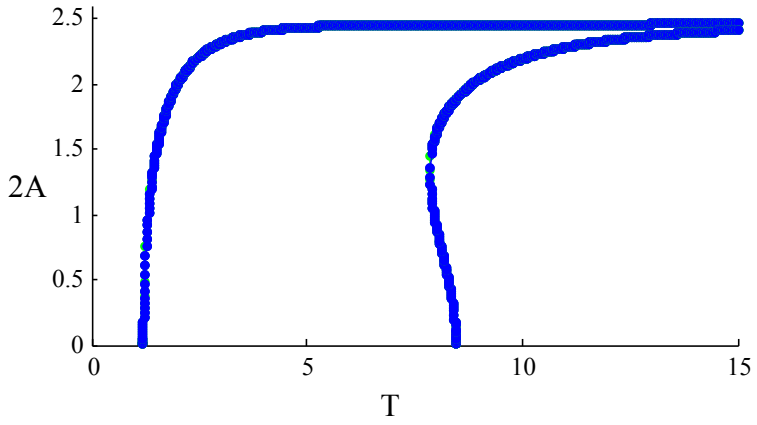

Figure 3.11: DDE-BIFTOOL plots of the limit cycles created by the first two Hopf bifurcations at $x = 0$, found for $\alpha = 0.5$ and increasing T.

For large delay T, we found square waves of higher frequency also existed. The periods of these higher order square waves are given by $\frac{2T}{2n-1}$, where n is an integer and $n = 1$ corresponds to the base square wave previously analyzed. See for example Fig. 3.12 which shows a higher order square wave for which $T = 100$, $\alpha = -0.75$ and $n = 2$.

Note that the amplitude of this square wave is the same as that of the base square wave, namely $A = \sqrt{\alpha + 1} = \sqrt{-0.75 + 1} = 1/2$. Note also that both the $n = 2$ higher order square wave of Fig. 3.12 and the base square wave of Fig. 3.9 coexist, each of them corresponding to different initial conditions. In fact, higher order square waves corresponding to larger values of n also coexist. An open question is what is the maximum value of n for which higher order square

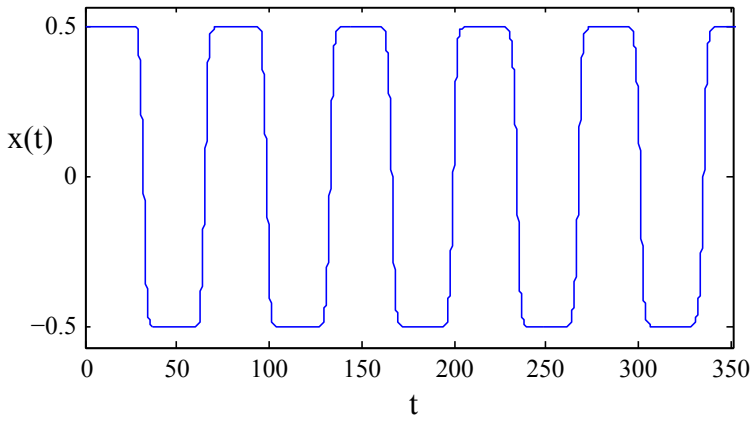

Figure 3.12: A higher order square wave for $T = 100$, $\alpha = -0.75$ and $n = 2$. Compare with the base square wave ($n = 1$) in Fig. 3.9

waves exist? (The problem is that as n increases, the period $\frac{2T}{2n-1}$ get smaller, and the assumption that the period is large compared to the jump time is no longer valid.)

Each edge of this square wave has length equal to half the period, $\frac{T}{2n-1}$. An analysis similar to that presented above in the section on large delay, for the base case, can be repeated here.

3.7 Conclusions

In this work we have shown that the diverse nature of the observed dynamics of the delay limit cycle oscillator with self-feedback, eq. (3.4), depends on the values of the parameters T and α. This may be illustrated by reference to various regions of the $\alpha - T$ parameter plane. See Fig. 3.13, where the five regions I, II, III, IV, V are bounded by curves a, b, c, d. Figure 3.14 shows a schematic of the amplitudes of steady–state motions as a function of α for a constant $T > 1$,

thereby crossing through regions I, II, III, and IV.

- Curve a is given by the Hopf condition eq. (3.11), so that a stable limit cycle is born as we cross from region I to region II.
- Curve b is simply $\alpha = 1$, and as we pass from region II to region III, a new pair of equilibrium points are born in a pitchfork bifurcation, see Fig. 3.1.
- Curve c is given by the Hopf condition eq. (3.15), so that an unstable limit cycle is born in a subcritical Hopf as we cross from region III to IV.
- Curve d is a limit cycle fold, see Fig. 3.7. As we cross from region IV to region V, a stable limit cycle disappears in a fold. Thus region V contains only the three equilibrium points, namely the origin (unstable) and the arms of the pitchfork (stable).
- Finally, the pitchfork equilibria disappear as we cross from region V to region I.

In summary, we may list the stable dynamical structures which appear in the five regions as follows:

- Region I contains a stable equilibrium at the origin.
- Regions II and III contain a stable limit cycle (which was born in a Hopf off the origin).
- Region IV contains both a stable limit cycle and a pair of stable equilibria (the arms of the pitchfork).
- Region V contains a pair of stable equilibria (the arms of the pitchfork).

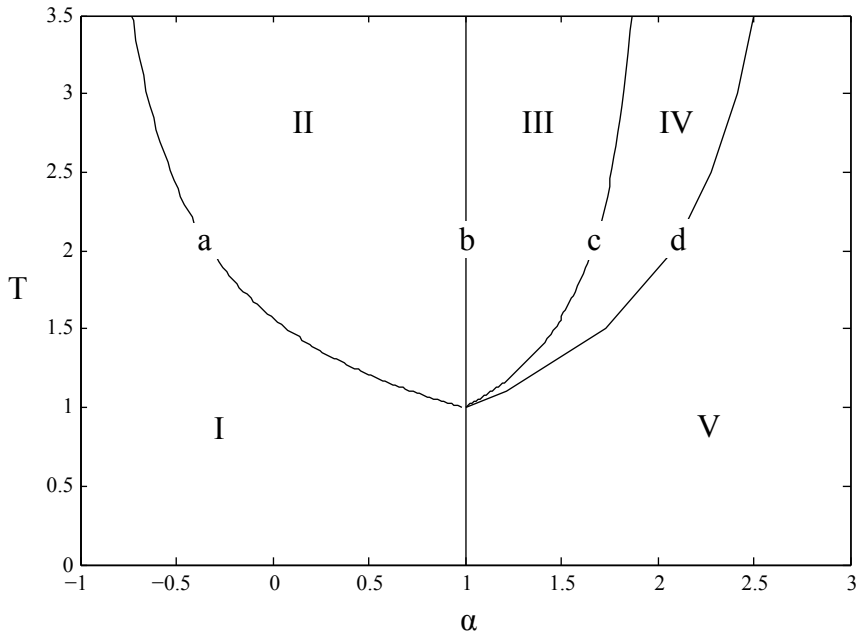

Figure 3.13: Regions of $\alpha - T$ parameter space and the bifurcation curves which bound them.

It is to be noted that the foregoing summary has omitted unstable motions (see Fig. 3.10) as well as motions occurring for large delay (see Figs. 3.9, 3.12).

As discussed in the Introduction, the delay limit cycle oscillator with self-feedback, eq. (3.4), investigated in this paper, is a special solution (the in-phase mode) of the system (3.2), (3.3). Another special solution is the out-of-phase mode, $x(t) = -y(t)$, governed by the equation:

$$\dot{x} = -x(t - T) - x^3 - \alpha x \tag{3.27}$$

Eq. (3.27) is seen to be identical to eq. (3.4) but with α replaced by $-\alpha$.

Both the in-phase and out-of-phase motions lie in invariant manifolds. If the system is given a general initial condition, numerical simulation has shown that

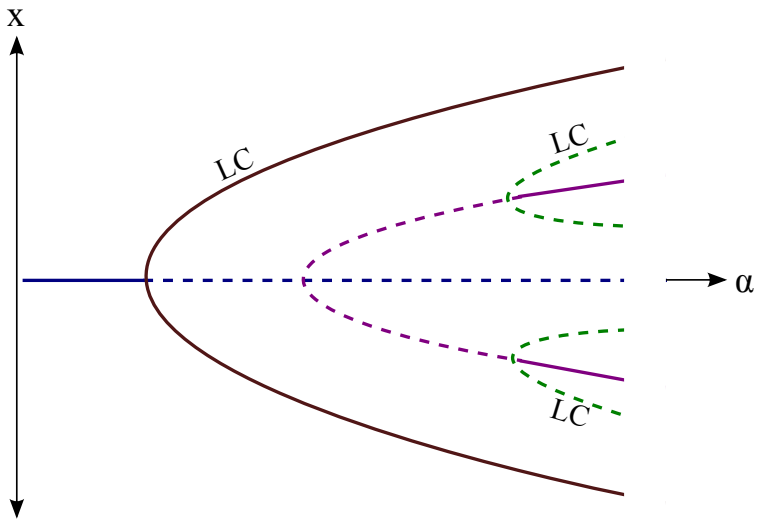

Figure 3.14: Schematic of equilibrium points and limit cycles seen for $T > 1$ with varying α. The behaviors change as the system crosses the supercritical Hopf (equation 3.11), pitchfork bifurcation ($\alpha = 1$) and subcritical Hopf (equation 3.15). Limit cycle fold not shown.

the resulting motion will approach one or the other of these invariant manifolds. A question which we are currently investigating concerns the stability of these manifolds as a function of the parameters T and α.

Eq. (3.1), the basic delay limit cycle oscillator upon which this work is based ([24],[25]), is perhaps the simplest example of a system which oscillates due to delay and nonlinearity. We look forward to further investigations based on this system.

CHAPTER 4

DYNAMICS OF AN OSCILLATOR WITH DELAY PARAMETRIC EXCITATION

4.1 Abstract

This paper involves the dynamics of a delay limit cycle oscillator being driven by a time–varying perturbation in the delay:

$$\dot{x} = -x\left(t - T(t)\right) - \epsilon x^3$$

with delay $T(t) = \frac{\pi}{2} + \epsilon k + \epsilon \cos \omega t$. This delay is chosen to periodically cross the stability boundary for the $x = 0$ equilibrium in the constant–delay system.

For most of parameter space, the system is nonresonant, leading to quasiperiodic behavior. However, a region of 2:1 resonance is shown to exist where the system's response frequency is entrained to half of the forcing frequency ω. By a combination of analytical and numerical methods, we find that the transition between quasiperiodic and entrained behavior consists of a variety of local and global bifurcations, with corresponding regions of multiple stable and unstable steady–states.

4.2 Introduction

A recent study [30] of dynamical systems with delayed terms has considered the following "delay limit cycle oscillator" in the form of a differential–delay

equation (DDE):

$$\dot{x} = -x(t - T_0) - \epsilon x^3 \tag{4.1}$$

This system exhibits a supercritical Hopf bifurcation at delay $T_0 = \pi/2$ such that the equilibrium point at the origin $x = 0$ is stable for $T_0 < \pi/2$ and unstable otherwise. The stable limit cycle for $T_0 > \pi/2$ is created with natural frequency 1 [24],[25],[7]. For an introduction to DDEs, see [31].

Equation (4.1) with $\epsilon = 0$ has had application to insect locomotion [32].

This paper considers a system of the same form as eq. (4.1), but with a periodically time–varying delay $T(t) = \pi/2 + \epsilon k + \epsilon \cos \omega t$:

$$\dot{x} = -x(t - T(t)) - \epsilon x^3 = -x\left(t - \frac{\pi}{2} - \epsilon k - \epsilon \cos \omega t\right) - \epsilon x^3 \tag{4.2}$$

The delay T is taken to be time–dependent such that the system may periodically cross the Hopf bifurcation exhibited by the constant T case. This causes the stability of the $x = 0$ equilibrium to regularly alternate between stable and unstable. We would anticipate the equilibrium being stable if it is in the stable region for more than half of the forcing period, and unstable otherwise. However, we will show that the effect of this forcing may cause unexpected behavior due to resonance between the forcing frequency ω and the frequency of the limit cycle created in the Hopf.

The effect of time–periodic delay on an oscillator has been studied with application to turning processes with varying spindle speed in machine–cutting [33].

4.3 Non–Resonant Two–Variable Expansion

We begin by expanding the system about the $\epsilon = 0$ solution, using two time variables, fast time u and slow time v:

$$u = t \qquad v = \epsilon t \qquad x = x_0 + \epsilon x_1 + O(\epsilon^2) \tag{4.3}$$

The multiple time scales lead to the restatement of the derivative:

$$\dot{x} = \frac{dx}{dt} = \frac{\partial x}{\partial u}\frac{du}{dt} + \frac{\partial x}{\partial v}\frac{dv}{dt} = x_u + \epsilon x_v \tag{4.4}$$

The delay term is also approximated by its Taylor expansion:

$$\begin{aligned} x_d &= x\,(u - T,\ v - \epsilon T) \\ &= x\left(u - \frac{\pi}{2},\ v\right) - \epsilon(k + \cos\omega u)x_u\left(u - \frac{\pi}{2},\ v\right) \\ &\quad -\epsilon\frac{\pi}{2}x_v\left(u - \frac{\pi}{2},\ v\right) + O(\epsilon^2) \end{aligned} \tag{4.5}$$

Within the original equation with these expansions applied, we can find the coefficients of each power of ϵ. The O(1) terms ($\epsilon = 0$) give the differential equation:

$$x_{0u} + x_0\left(u - \frac{\pi}{2},\ v\right) = 0 \tag{4.6}$$

with a solution of the form:

$$x_0(u, v) = A(v)\cos u + B(v)\sin u \tag{4.7}$$

The $O(\epsilon)$ terms are found from the original (expanded) equation to give an equation for x_1:

$$\begin{aligned} x_{1u} + x_1\left(u - \frac{\pi}{2},\ v\right) &= -x_{0v} + (k + \cos\omega u)x_{0u}\left(u - \frac{\pi}{2},\ v\right) \\ &\quad +\frac{\pi}{2}x_{0v}\left(u - \frac{\pi}{2},\ v\right) - x_0^3 \end{aligned} \tag{4.8}$$

Since we will be looking to eliminate secular terms $\cos(u)$ and $\sin(u)$, at this point we note that some terms' resonance or nonresonance are dependent on the value of ω, in particular:

$$\begin{aligned}(\cos\omega u)(A\cos u + B\sin u) &= \frac{A}{2}(\cos(\omega+1)u + \cos(\omega-1)u) \\ &\quad + \frac{B}{2}(\sin(\omega+1)u - \sin(\omega-1)u) \end{aligned} \tag{4.9}$$

Here we will split our analysis into two cases, resonant ($\omega \approx 2$) and non–resonant ($\omega \not\approx 2$), in order to account for the presence or absence of the resonant terms that arise from $\cos\omega u$.

4.3.1 Non–Resonant Behavior

Eliminating secular terms in the case where $\omega \not\approx 2$ results in the approximation and slow flow:

$$(2\pi^2+8)A' = 8kA - 4\pi kB + (3\pi B - 6A)(A^2+B^2) \tag{4.10}$$

$$(2\pi^2+8)B' = 8kB + 4\pi kA - (3\pi A + 6B)(A^2+B^2) \tag{4.11}$$

Transforming to polar form by taking $A = R\cos\theta$ and $B = R\sin\theta$, to result in the new form $x_0(u,v) = R(v)\cos(u-\theta(v))$, gives:

$$(\pi^2+4)R' = R(4k - 3R^2) \tag{4.12}$$

$$(2\pi^2+8)\theta' = \pi(4k - 3R^2) \tag{4.13}$$

The R' equation is uncoupled, allowing us to study it separately. $R = 0$ solves $R' = 0$ for all parameter values (representing the origin $x = 0$); this solution is stable for all $k < 0$. For $k > 0$ the stable solution is $R = 4k/3$, with a corresponding

$\theta' = 0$. Based on this result, $x(t)$ is approximated to have response frequency 1 for $k > 0$, as in the original limit cycle oscillator eq. (4.1) with $T_0 > \pi/2$.

We note that in this expansion, the periodic forcing is shown to have no effect to this order. By expanding about the resonant forcing frequency $\omega = 2$ below, we will see that the second frequency does have an effect on the non–resonant behavior as well as behavior within the resonant region.

4.4 Resonant Two–Variable Expansion

According to eq. (4.9), the choice $\omega = 2$ makes the system resonant. To consider this behavior, we will redefine the two–variable expansion about this value by defining $\omega = 2 + \epsilon\Delta$.

Using new variables for fast time ξ and slow time η to expand about the resonance at $\omega = 2$:

$$\omega t = 2\xi = 2(1 + \epsilon\Delta/2)t \qquad \eta = \epsilon t \tag{4.14}$$

$$\dot{x} = \frac{dx}{dt} = \frac{\partial x}{\partial \xi}\frac{d\xi}{dt} + \frac{\partial x}{\partial \eta}\frac{d\eta}{dt} = (1 + \epsilon\Delta/2)x_\xi + \epsilon x_\eta \tag{4.15}$$

we proceed as before. The x_0 solution takes the same form as eq. (4.7) in terms of the new time variables:

$$x_0(\xi, \eta) = A(\eta)\cos\xi + B(\eta)\sin\xi \tag{4.16}$$

while the $O(\epsilon)$ terms give the following equation for x_1:

$$\begin{aligned} x_{1\xi} + x_1\left(\xi - \frac{\pi}{2},\ \eta\right) &= -x_{0\eta} - \frac{\Delta}{2}x_{0\xi} + \left(\frac{\pi\Delta}{4} + k + \cos 2\xi\right)x_{0\xi}\left(\xi - \frac{\pi}{2},\ \eta\right) \\ &\quad + \frac{\pi}{2}x_{0\eta}\left(\xi - \frac{\pi}{2},\ \eta\right) - x_0^3 \end{aligned} \tag{4.17}$$

Within the resulting equation, we choose $A(\eta)$ and $B(\eta)$ to eliminate secular terms by collecting the coefficients of the $\sin(\xi)$ and $\cos(\xi)$ terms. This results in the following system of ordinary differential equations as the slow flow of the system:

$$(2\pi^2 + 8)A' = (8k + 4)A + (2\pi - 4\pi k - \pi^2\Delta - 4\Delta)B + (-6A + 3\pi B)(A^2 + B^2) \quad (4.18)$$

$$(2\pi^2 + 8)B' = (2\pi + 4\pi k + \pi^2\Delta + 4\Delta)A + (8k - 4)B + (-6B - 3\pi A)(A^2 + B^2) \quad (4.19)$$

where we have used $x_0(\xi - \pi/2, \eta) = -x_{0\xi}$ from the $O(1)$ terms to simplify the delay terms in eq. (4.17). We note that eqs. (4.18) and (4.19) are similar to the non–resonant slow flow eqs. (4.10) and (4.11), but include additional terms caused by the resonance with the parametric forcing term.

This system of slow flow equations exhibits an assortment of bifurcation phenomena. Its steady–state solutions will include equilibrium points, representing periodic motions in $x(t)$, and limit cycles, corresponding to quasiperiodic behavior of the original system.

4.5 Slow Flow Equilibria

Equilibria in the slow flow solve $A' = B' = 0$. We use Maxima to eliminate B and obtain a single expression $f(A) = 0$, then additionally require $f'(A) = 0$ to find double roots in A, which will include pairs of equilibrium points coalescing in saddle–node bifurcations.

Eliminating A from these equations results in multiple expressions representing curves in $\Delta - k$ parameter space. The following locations in parameter

space are observed to correspond to double roots in (A, B):

$$16k^2 + 8\pi\Delta k + (\pi^2 + 4)\Delta^2 = 4 \tag{4.20}$$

$$\Delta = \pm 1 \tag{4.21}$$

Equation (4.20) is an ellipse which may be shown to represent a pair of pitchfork bifurcations off of $A = B = 0$. Equation (4.21) represents double saddle–node bifurcations away from the origin, transitioning between regions of 1 and 5 equilibria; this restricts them to k values above the ellipse. Together these bifurcation curves describe regions in parameter space with 1, 3, and 5 slow flow equilibria, as can be seen in Fig. 4.1.

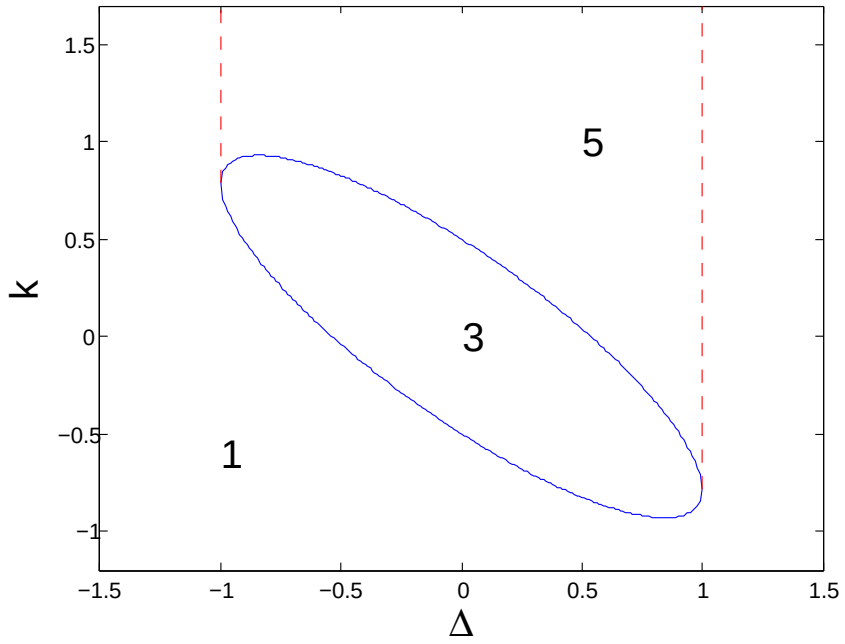

Figure 4.1: Regions with 1, 3, and 5 slow flow equilibria, bounded by (dashed) double saddle–node bifurcations and (solid) pitchfork bifurcations.

Results from AUTO bifurcation continuation software [13], used on the slow

flow for $k = -0.1$ and varying Δ, show the interaction of the equilibria as the system crosses these bifurcation curves (see Fig. 4.2).

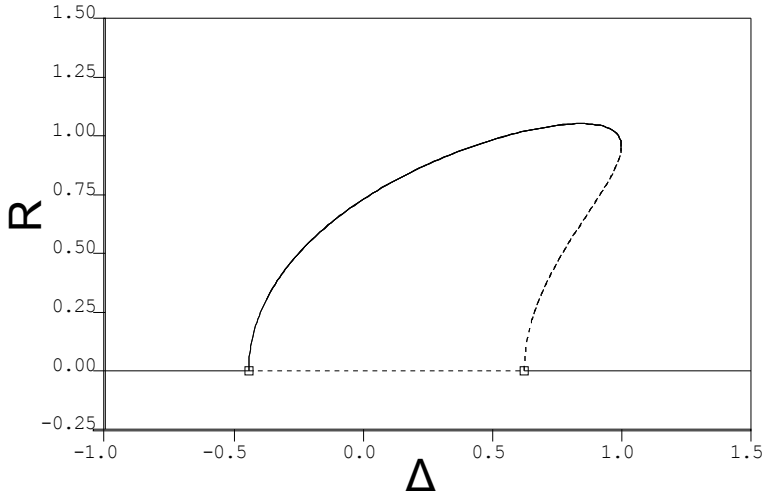

Figure 4.2: AUTO results for $k = -0.1$ with varying Δ. Plotting the amplitude $R = \sqrt{A^2 + B^2}$ of the $x(t)$ response for the equilibria, with stability information (solid is stable, dashed is unstable). All points on the $R \neq 0$ curve represent 2 equilibria by symmetry.

4.6 Stability of $x = 0$

The stability of the $x = 0$ solution is governed by the Jacobian matrix J for the slow flow about $A = B = 0$:

$$J = \begin{bmatrix} 8k + 4 & 2\pi - 4\pi k - (\pi^2 + 4)\Delta \\ 2\pi + 4\pi k + (\pi^2 + 4)\Delta & 8k - 4 \end{bmatrix} \tag{4.22}$$

Since the eigenvalues λ of J satisfy the characteristic equation:

$$\lambda^2 - \mathrm{tr}(J)\lambda + \det(J) = 0 \tag{4.23}$$

the condition for stability $\mathrm{Re}(\lambda) < 0$ requires both $\det(J) > 0$ and $\mathrm{tr}(J) < 0$ [34].

The stability boundary $\det(J) = 0$ gives eq. (4.20) and corresponds to the ellipse in Fig. 4.1. The inside of the ellipse gives $\det(J) < 0$ such that the origin is a saddle point and therefore unstable.

Outside the ellipse where $\det(J) > 0$, the stability of the origin depends on the sign of $\mathrm{tr}(J) = 16k$. At the stability boundary $\mathrm{tr}(J) = 0$, the eigenvalues λ are purely imaginary leading to a Hopf bifurcation. Thus the origin $A = B = 0$ undergoes a Hopf bifurcation at $k = 0$ under the condition which restricts to the outside of the ellipse:

$$\Delta^2 > 1/(\pi^2 + 4) \tag{4.24}$$

At the Hopf bifurcation, the eigenvalues $\lambda = iW$ give the response frequency to be:

$$W = \sqrt{(\pi^2 + 4)^2\Delta^2 - 4(\pi^2 + 4)} \tag{4.25}$$

in slow time η, or frequency ϵW in t.

These conditions on the determinant and trace, together with the corresponding pitchfork and Hopf bifurcation curves, lead to the stability regions seen in Figure 4.3.

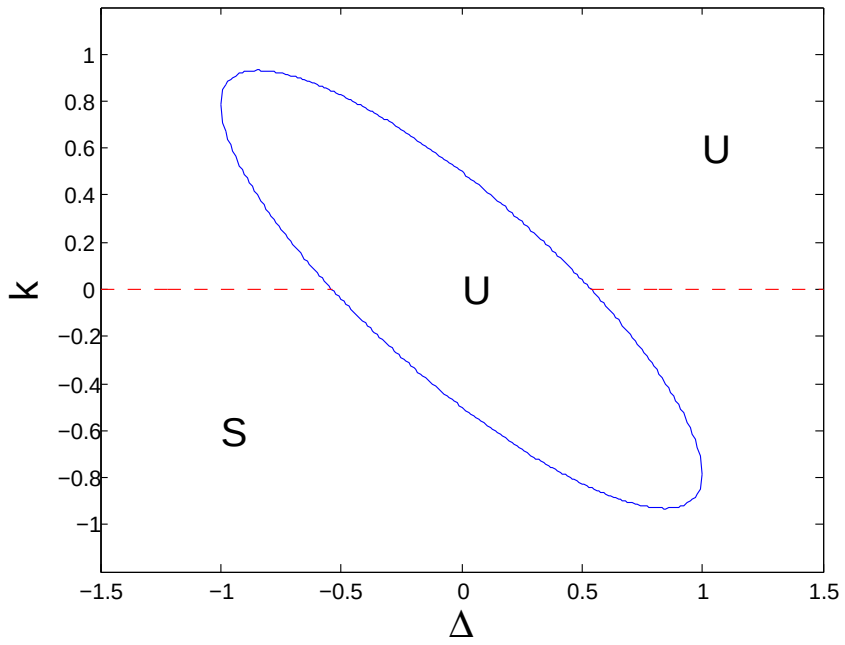

Figure 4.3: Stability of $x = 0$ near the resonance; "U" is unstable, "S" is stable. Changes in stability are caused by pitchfork bifurcations (solid line) and Hopf bifurcations (dashed line).

4.7 The Limit Cycle from $k = 0$ Hopf

The Hopf bifurcation off the origin at $k = 0$ is found to be supercritical, resulting in a stable limit cycle in the slow flow for $k > 0$ for values of Δ satisfying eq. (4.24), i.e. outside the ellipse. This limit cycle represents a quasiperiodic motion in the overall system, on account of the two frequencies represented: the original Hopf frequency ϵW and the halved forcing frequency $\omega/2 = 1 + \epsilon\Delta/2$.

We will show that this limit cycle is destroyed as the system parameters move into the resonance region (i.e. as $\omega \to 2$ or $\Delta \to 0$).

4.8 Stability of $x \neq 0$ Slow Flow Equilibria

Just as for the $A = B = 0$ equilibrium above, we consider the linear stability of the nontrivial equilibria of the slow flow by linearizing about their locations [34]. The pair of equilibria found in both the regions of 3 and 5 equilibria (see Fig. 4.1) have the locations:

$$A_m = \pm\sqrt{\left(\frac{2k}{3}+\frac{\pi\Delta}{6}+\frac{1}{3}\right)\left(1+\sqrt{1-\Delta^2}\right)-\frac{\Delta^2}{3}} \tag{4.26}$$

$$B_m = \mp\sqrt{\left(\frac{2k}{3}+\frac{\pi\Delta}{6}-\frac{1}{3}\right)\left(1-\sqrt{1-\Delta^2}\right)+\frac{\Delta^2}{3}} \tag{4.27}$$

By linearizing about this location and looking for pure imaginary eigenvalues, we find that these equilibria change stability in Hopf bifurcations on the curve:

$$k = -\sqrt{1-\Delta^2}-\frac{\pi\Delta}{2} \tag{4.28}$$

This curve intersects with the ellipse when $k = 0$ and therefore only exists for $k > 0$. It reaches an end by approaching $\Delta = -1$ tangentially as k approaches $\pi/2$.

In contrast, the pair of equilibria which exist only in the region of 5 equilibria (see Fig. 4.1):

$$A_p = \pm\sqrt{\left(\frac{2k}{3}+\frac{\pi\Delta}{6}+\frac{1}{3}\right)\left(1-\sqrt{1-\Delta^2}\right)-\frac{\Delta^2}{3}} \tag{4.29}$$

$$B_p = \mp\sqrt{\left(\frac{2k}{3}+\frac{\pi\Delta}{6}-\frac{1}{3}\right)\left(1+\sqrt{1-\Delta^2}\right)+\frac{\Delta^2}{3}} \tag{4.30}$$

are found to be unstable saddle points wherever they exist.

The foregoing discussion of stability of the nontrivial equilibria is summarized in Fig. 4.4.

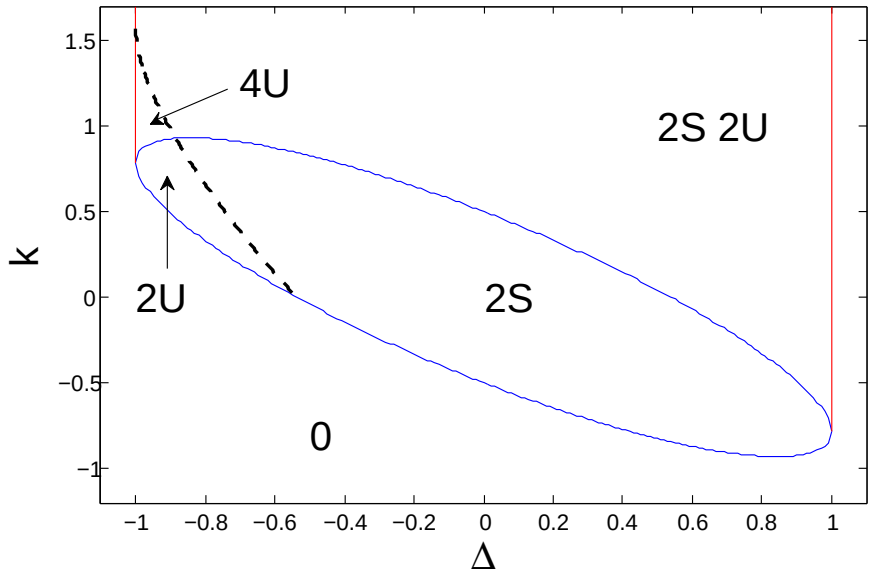

Figure 4.4: Numbers of Stable/Unstable nontrivial equilibria (that is, besides $A = B = 0$). Ellipse is the set of pitchfork bifurcations (eq. (4.20)). Vertical lines are double saddle–node bifurcations (eq. (4.21)). The dashed curve is a Hopf bifurcation (eq. (4.28)).

4.9 Slow Flow Phase Portraits

So far we have considered local bifurcations (pitchfork, saddle–node, Hopf) as seen in Figs. 4.3 and 4.4. Figure 4.5 shows these bifurcations along with the global bifurcations that we will now discuss, being limit cycle folds and heteroclinic bifurcations.

We use Matlab to plot numerically–obtained phase portraits of the slow flow eqs. (4.18) and (4.19). Figure 4.6 is a zoom of the left half of Fig. 4.5 with regions labeled corresponding to phase portraits in Fig. 4.7.

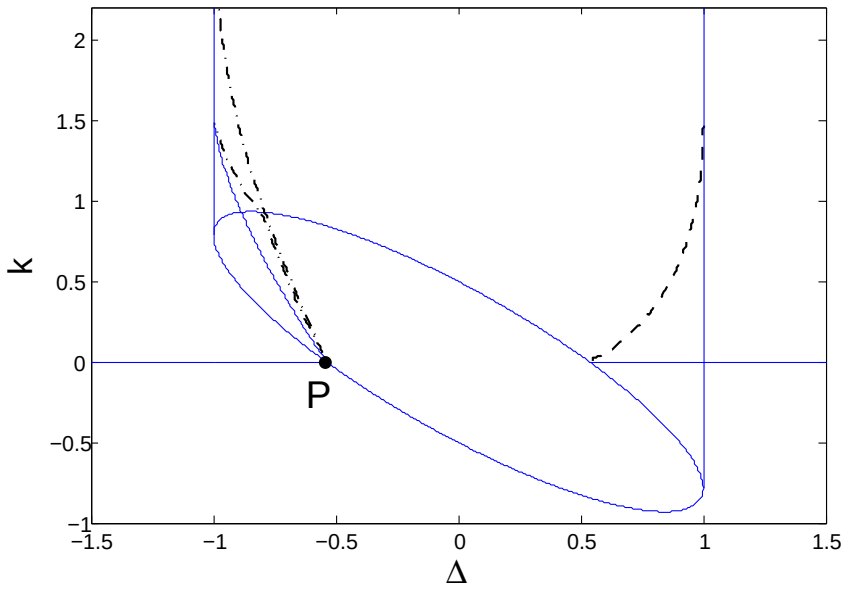

Figure 4.5: Local bifurcation curves (solid lines) as seen in Figs. 4.3 and 4.4. Global bifurcation curves (dashed lines) found numerically. Degenerate point P also marked, see Fig. 4.8.

Figure 4.8 shows a schematic of the bifurcation curves in the neighborhood of point P. Along with the phase portraits in Figs. 4.7(a-f), this diagram is comparable to those found in Figs. 7.3.7 and 7.3.9 of [34], which describe a Takens-Bogdanov bifurcation with rotational symmetry. (We note that this rotational symmetry is consistent with our slow flow equations (4.18) and (4.19), which are symmetric under the transformation $A \to -A$, $B \to -B$.)

Figure 4.9 is a zoom of the right half of Fig. 4.5 with regions labeled corresponding to phase portraits in Fig. 4.10.

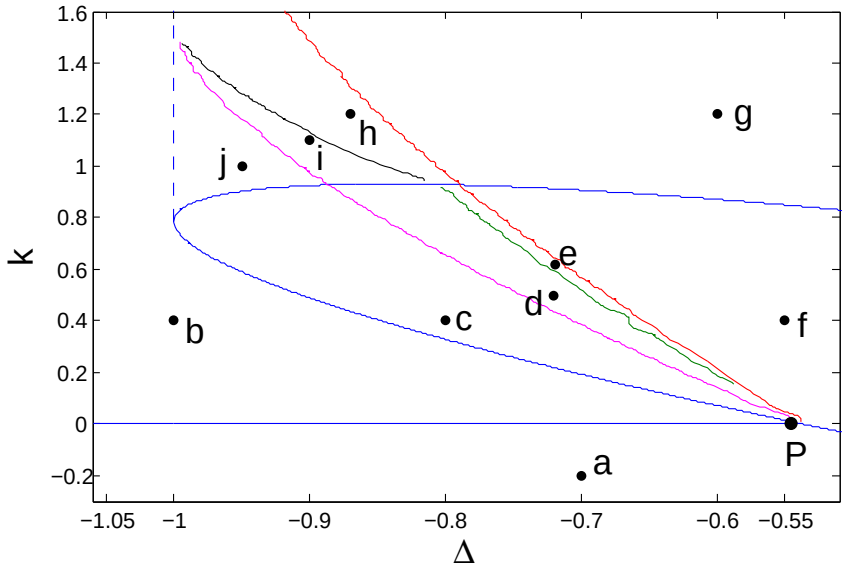

Figure 4.6: Zoom of Fig. (4.5) with labeled points explored in Fig. 4.7. The degenerate point P is explored in Fig. 4.8.

4.10 Stable Motions of Eq. (4.2)

The previous figures (Figs. 4.1-4.10) correspond to the behaviors of the slow flow equations (4.18) and (4.19). Now we summarize the corresponding stable motions $x(t)$ in the original system eq. (4.2). (Unstable motions are not mentioned since they will not be seen in simulations.)

- Region a: origin only, $x = 0$ (no oscillation)
- Regions f, g: entrained motion only
- Region b, c, j: quasiperiodic (unentrained) motion only
- Regions d, e, h, i, r: quasiperiodic and entrained motions
- Region s: origin $x = 0$ (no oscillation) and entrained oscillation

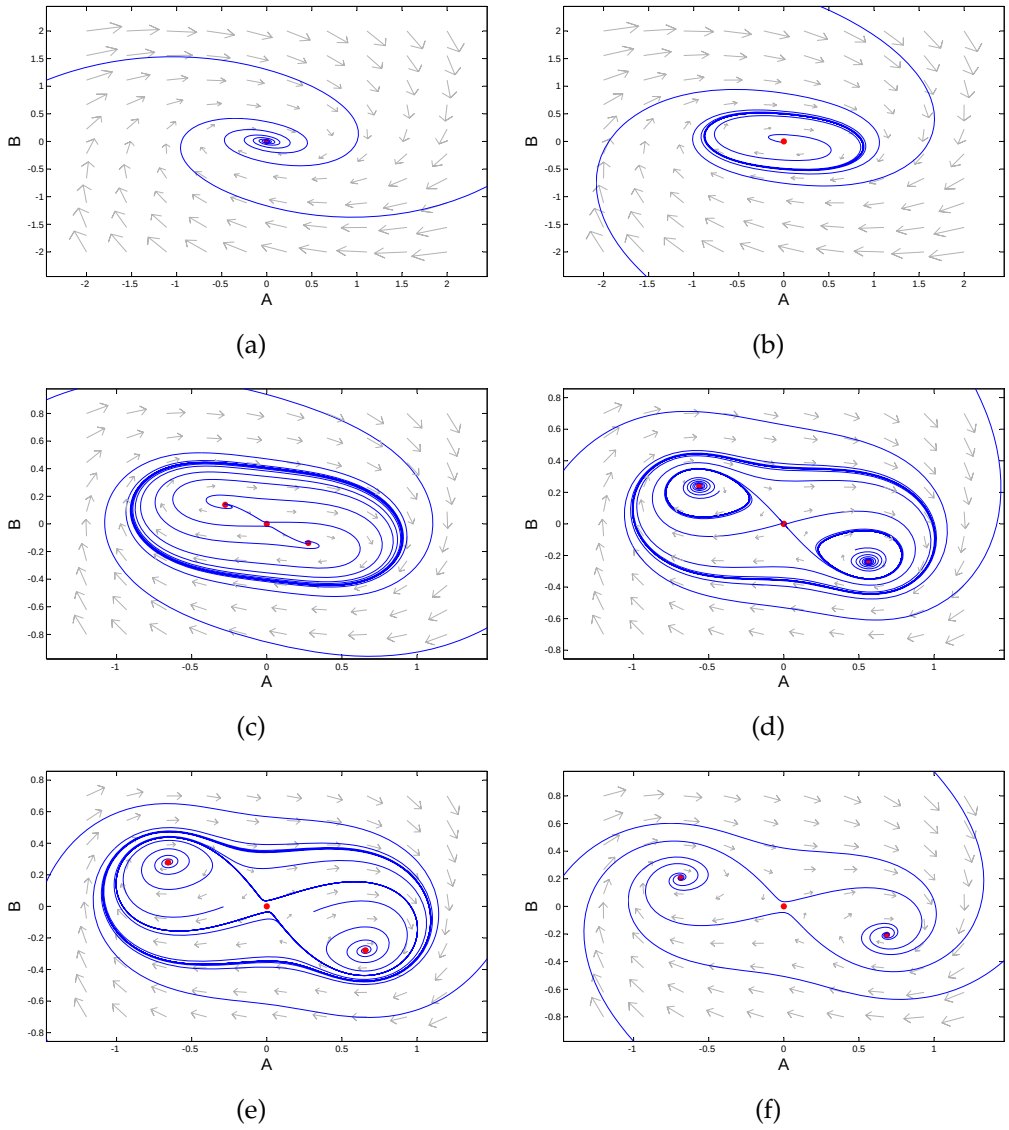

Figure 4.7: Representative phase portraits of the slow flow from each region of parameter space, locations as marked in Fig. (4.6). Obtained with numerical integration via `pplane`.

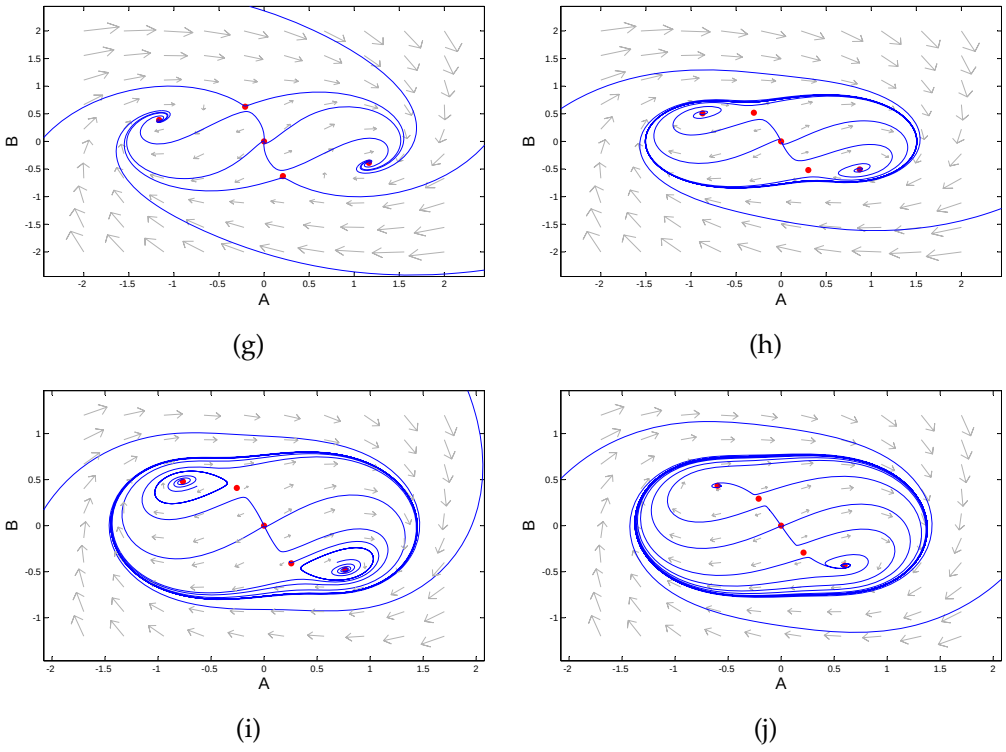

Figure 4.7: (continued)

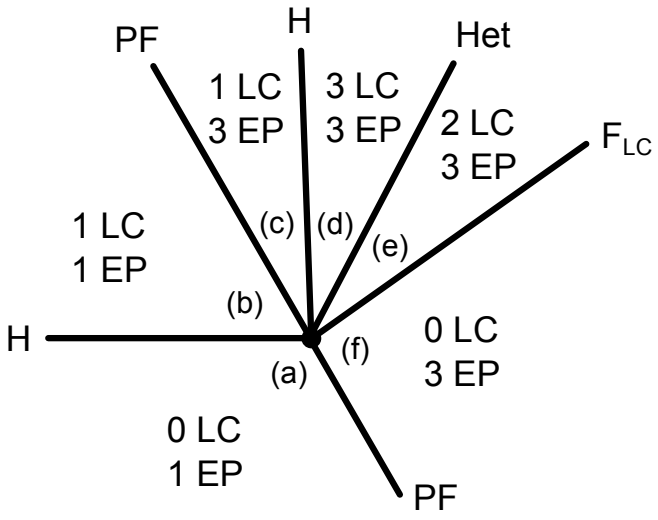

Figure 4.8: Schematic at degenerate point P from Figs. 4.5 and 4.6, showing the number of limit cycles (LC) and equilibrium points (EP) in each labeled region. Bifurcation types also shown: Hopf (H), pitchfork (PF), heteroclinic (Het), and limit cycle fold (F_{LC}).

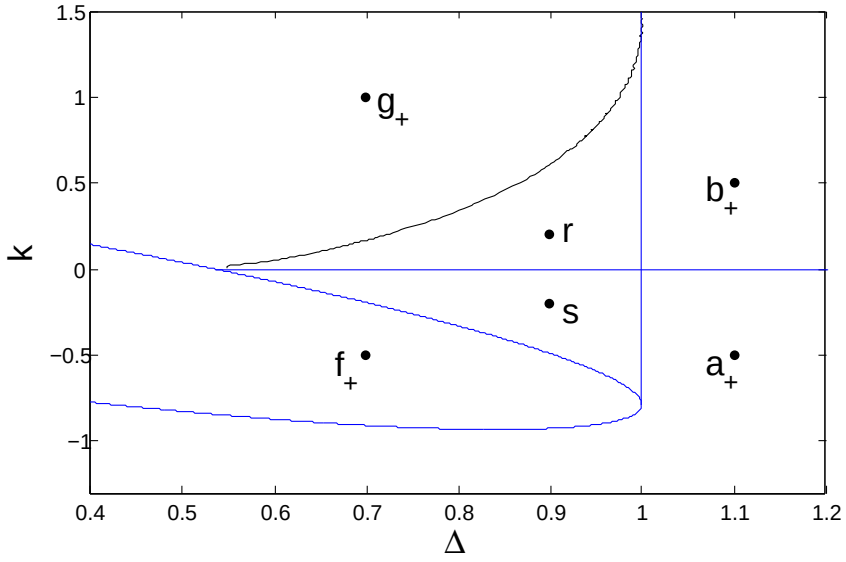

Figure 4.9: Zoom of Fig. (4.5) with labeled points. Points a_+, b_+, f_+, and g_+ are qualitatively identical to points a, b, f, and g respectively from Fig. (4.6).

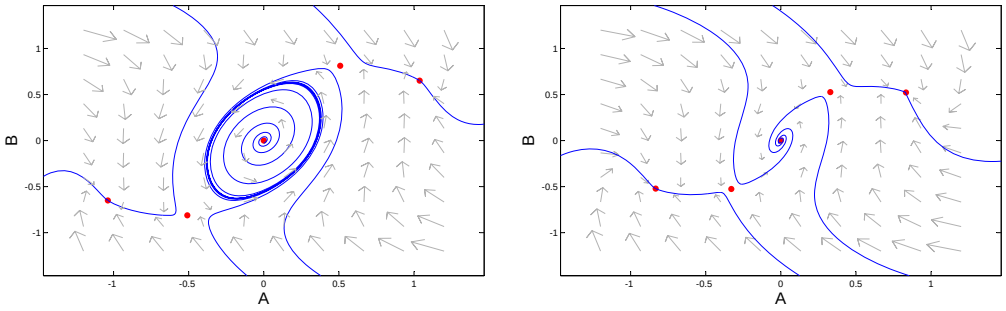

(r) (s)

Figure 4.10: Representative phase portraits of the slow flow from regions of parameter space, locations as marked in Fig. (4.9). Obtained with numerical integration via `pplane`.

We note that in the regions with multiple stable solutions, the basins of attraction for each stable behavior are defined by initial conditions which are functions of time.

4.11 Conclusions

In this work, we considered the dynamics of a delay limit cycle oscillator whose delay is varied periodically across a critical value of the delay corresponding to a Hopf bifurcation, such that the equilibrium solution $x = 0$ alternates in time between being stable and unstable.

For most forcing frequencies of the delay, the equilibrium at the origin $x = 0$ is stable provided the average delay is smaller than the critical delay. If the average delay is larger than the critical delay, the system exhibits quasiperiodic behavior due to the coappearance of oscillations at the forcing–frequency along with oscillations at the limit cycle frequency.

However, the system has a 2:1 resonance which results in a small region of parameter space about $\omega = 2$ where the oscillator behaves periodically. Within this region, the system is entrained to oscillate at half of the forcing frequency, see Fig. 4.11. We conjecture that other resonances (m:n) exist in this problem just as they do in Mathieu's equation [24], but we have not found them analytically or numerically as yet.

Within the transition between resonance and non–resonance, the system is found to have regions of multiple stable behaviors (periodic and quasiperiodic motions). Each steady–state has its own basin of attraction, and the long–term

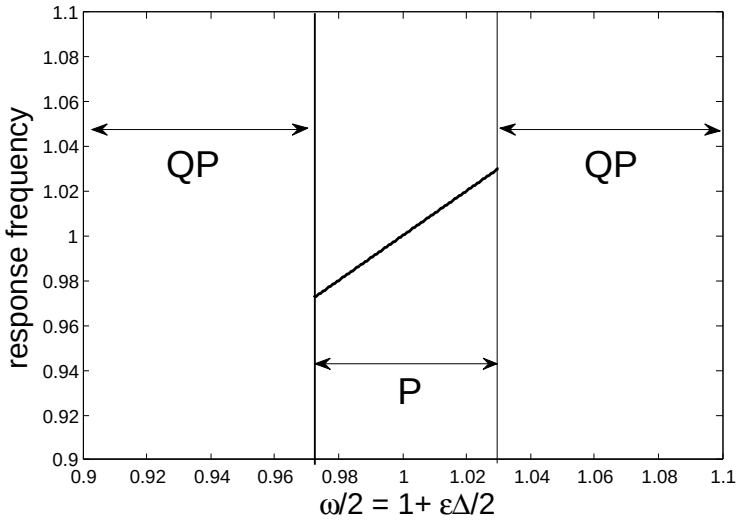

Figure 4.11: The system is entrained to periodic motion (P) at frequency $\omega/2$ within the resonance region (shown for $k = 0.05$). It exhibits quasiperiodic motion (QP) with multiple frequencies everywhere else.

behavior is then determined by the initial conditions on $x(t)$. (These initial conditions consist of functions of time for a differential–delay equation.)

This system represents a particular form of parametric excitation which has been previously unstudied, where the periodic forcing term appears in the delay. A remarkably similar bifurcation set has been observed in systems which did not involve delay [35],[36],[37]. Each of these studies involves a system undergoing a Hopf bifurcation which is being forced parametrically: in [35], the system is represented as a second–order differential equation; in [36] and [37], as a first–order differential equation on the complex plane.

CHAPTER 5

ADDITIONAL DISCUSSION AND CONCLUSIONS

Within the previous chapters, we have considered three oscillator problems with varied coupling or driving terms.

5.1 Coupled and Driven Phase-Only Oscillators

In Chapter 2 we discussed a pair of coupled oscillators which are also driven by a third oscillator.

Despite the three distinct frequencies in the system, for large enough driving strength, the oscillators lock to the driver's frequency. The minimum driving strength for full locking is largest for zero coupling, being the strength needed to lock both oscillators individually. As coupling strength increases, the pair of oscillators lock to each other at the average of their original frequencies, and the critical driving strength asymptotically approaches the value needed to lock an oscillator with that average frequency. That is, the system is more easily locked to the driver when the oscillators are coupled than when they are independent of each other. While this is useful from the perspective of the driving oscillator, it might be considered a detriment to the design of systems which are meant to sychronize internally while ignoring external influence.

Within the "drift" region of parameter space we found resonances between the coupled pair such that their average frequencies are rationally related to each other. This includes the large-coupling scenario where they are 1:1 locked with each other, but other ratios are also possible within specific regions of parameter space. The methods used to find these m:n resonances are limited by

the accuracy of our numerical integrations and how fine of a mesh of parameter values can be reasonably chosen. The 1:1, 2:1, and similarly low-valued resonances are relatively straightforward to find, due to the simple ratios and the parameter regions being wide. However, the regions of m:n resonances with larger m and n will be smaller (since the resonances are weaker) and therefore more difficult to find.

Since this system's driver is expected to relate to environmental/external forcing on a coupled oscillator system, there are several ways that this system could be made more relevant to mechanical systems. We would hope to consider more realistic oscillator models in the same scenario, but also other external factors such as delay in the coupling terms, non-sinusoidal noise, and other forms of coupling or driving.

5.2 Delay Limit Cycle Oscillator under Self-Feedback

Chapter 3 explored the in-phase and out-of-phase invariant manifolds of a coupled pair of identical oscillators. Behavior of the system on these manifolds was studied as a single oscillator with an instantaneous self-feedback term.

Increasing the strength of the self-feedback term was found to cause the oscillator's stable limit cycle to disappear in a limit cycle fold. Beyond the limit cycle fold, the system would no longer oscillate, but would instead settle onto a stable non-trivial equilibrium solution. In this way the self-feedback term was found to interfere with the oscillation rather than to resonate with it.

For large delay, the stable oscillations approach the form of square waves.

Square wave oscillations of multiple frequencies were found numerically, suggesting that each of them is stable for a certain group of initial conditions (which are given as functions of time). This high number of overlapping limit cycles is possible due to the infinite-dimensionality of delay differential equations.

Unfortunately, very little may be said at this point regarding analysis of the many global bifurcations in this problem. Of particular interest would be the limit cycle fold that marks the disappearance of the stable oscillation, since there are several other steady-state behaviors (both stable and unstable) present in the system for those parameter values.

In the problem's original context, further analysis is needed regarding the stability of the invariant manifolds within the full system, beyond initial observations which suggest that their stability is dependent on the sign of the coupling term. An additional expansion upon this work would be to make the oscillators non-identical in the full system by perturbing their uncoupled frequencies or individual coupling strengths.

5.3 Parametric Excitation in Delay

The system considered in Chapter 4 was a delay limit cycle oscillator perturbed with a sinusoidal time-varying delay term.

The driving term in the delay caused the system to exhibit quasiperiodic motion for non-resonant parameter values. However, a region of 2:1 resonance between the driving frequency and the frequency of the unperturbed oscillator was discovered. The transition between the resonant and non-resonant regions

of parameter space was found to include several bifurcation curves and intermediate regions involving multiple stable behaviors.

Much of the difficulty of analyzing the global bifurcations of this system was mitigated by our use of perturbation methods. Since the delayed term was part of the unperturbed system, the slow flow for the oscillator could be written without delayed terms. (This was not as useful in the self-feedback problem of Chapter 3, since we did not choose to assume a weak feedback term.)

This problem was of particular interest due to the novel nature of the parametric excitation. In contrast to the model of parametric excitation as a non-constant coefficient on a linear term (such as in Mathieu's equation), the driving term in this system is a perturbation to the internal delay parameter. Despite this distinction, we found similarities to the traditional parametric excitation problem, particularly that the primary resonance is 2:1 (rather than 1:1) between the driving frequency and the natural frequency of the undriven system.

We have also been able to directly compare the rich set of bifurcations found in this system with those found in second-order systems of varying complexity without delay. Since many of these features appear to be common to multiple systems with parametric resonance across a Hopf bifurcation, it may be possible to generalize our results to other systems with similar nature.

APPENDIX A

HOPF BIFURCATION FORMULA FOR FIRST-ORDER DDES

In this Appendix we review the Hopf bifurcation formula, first derived in [26], for first-order constant-coefficient differential delay equations of the following form (as in eq. (3.16)):

$$\frac{du}{dt} = \gamma u + \beta u_d + a_1 u^2 + a_2 u u_d + a_3 u_d^2 + b_1 u^3 + b_2 u^2 u_d + b_3 u u_d^2 + b_4 u_d^3 \tag{A.1}$$

where $u = u(t)$ and $u_d = u(t - T)$.

The amplitude A of the approximate solution $u = A\cos\omega t$ is given by the expression:

$$A^2 = \mu P/Q \tag{A.2}$$

where

$$\begin{aligned} P = \quad & 4\beta^3(4\gamma - 5\beta)(\beta - \gamma)(\gamma + \beta)^2 \qquad (A.3)\\ Q = \quad & 5b_2T_H\beta^6 + 15b_4T_H\beta^6 + 15b_1\beta^5 + 5b_3\beta^5 - 4a_1^2T_H\beta^5 \\ & -3a_2^2T_H\beta^5 - 22a_3^2T_H\beta^5 - 7a_1a_2T_H\beta^5 - 14a_1a_3T_H\beta^5 \\ & -7a_2a_3T_H\beta^5 - 15\gamma b_1T_H\beta^5 + \gamma b_2T_H\beta^5 - 15\gamma b_3T_H\beta^5 \\ & +3\gamma b_4T_H\beta^5 - 18a_1^2\beta^4 - a_2^2\beta^4 - 4a_3^2\beta^4 - 9a_1a_2\beta^4 \\ & -18a_1a_3\beta^4 - 9a_2a_3\beta^4 + 3\gamma b_1\beta^4 - 15\gamma b_2\beta^4 + \gamma b_3\beta^4 \\ & -15\gamma b_4\beta^4 + 18\gamma a_1^2T_H\beta^4 + 7\gamma a_2^2T_H\beta^4 + 12\gamma a_3^2T_H\beta^4 \\ & +19\gamma a_1a_2T_H\beta^4 + 30\gamma a_1a_3T_H\beta^4 + 37\gamma a_2a_3T_H\beta^4 \\ & -3\gamma^2b_1T_H\beta^4 + 6\gamma^2b_2T_H\beta^4 - 3\gamma^2b_3T_H\beta^4 - 12\gamma^2b_4T_H\beta^4 \\ & +12\gamma a_1^2\beta^3 + 11\gamma a_2^2\beta^3 + 26\gamma a_3^2\beta^3 + 33\gamma a_1a_2\beta^3 \\ & +30\gamma a_1a_3\beta^3 + 19\gamma a_2a_3\beta^3 - 12\gamma^2b_1\beta^3 - 3\gamma^2b_2\beta^3 \end{aligned}$$

$$
\begin{aligned}
&+6\gamma^2 b_3\beta^3 - 3\gamma^2 b_4\beta^3 - 8\gamma^2 a_1^2 T_H\beta^3 - 12\gamma^2 a_2^2 T_H\beta^3 \\
&+4\gamma^2 a_3^2 T_H\beta^3 - 26\gamma^2 a_1 a_2 T_H\beta^3 - 16\gamma^2 a_1 a_3 T_H\beta^3 \\
&-20\gamma^2 a_2 a_3 T_H\beta^3 + 12\gamma^3 b_1 T_H\beta^3 + 2\gamma^3 b_2 T_H\beta^3 \\
&+12\gamma^3 b_3 T_H\beta^3 - 14\gamma^2 a_2^2\beta^2 - 8\gamma^2 a_3^2\beta^2 - 18\gamma^2 a_1 a_2\beta^2 \\
&-12\gamma^2 a_1 a_3\beta^2 - 32\gamma^2 a_2 a_3\beta^2 + 12\gamma^3 b_2\beta^2 + 2\gamma^3 b_3\beta^2 \\
&+12\gamma^3 b_4\beta^2 + 8\gamma^3 a_2^2 T_H\beta^2 + 8\gamma^3 a_1 a_2 T_H\beta^2 \\
&-4\gamma^3 a_2 a_3 T_H\beta^2 - 8\gamma^4 b_2 T_H\beta^2 + 4\gamma^3 a_2^2\beta \\
&-8\gamma^3 a_3^2\beta + 8\gamma^3 a_2 a_3\beta - 8\gamma^4 b_3\beta + 8\gamma^4 a_2 a_3
\end{aligned}
\tag{A.4}
$$

where ω and T_H are the values of frequency and delay associated with the Hopf, and where $\mu = T - T_H$.

In the case of the delay limit cycle oscillator with self-feedback, eq. (3.4), we have for the Hopf at $u = x = 0$:

$$
\begin{aligned}
\gamma &= \alpha \\
\beta &= -1 \\
a_1 &= a_2 = a_3 = 0 \\
b_1 &= -1 \\
b_2 &= b_3 = b_4 = 0
\end{aligned}
$$

and we have T_H given by eq. (3.15). When these parameter values are substituted into the above expressions for P and Q, we obtain eq. (3.17).

BIBLIOGRAPHY

[1] Rayleigh, L.: *The Theory of Sound*, p. 81. Dover Publications, Mineola (1945).

[2] van der Pol, B.: On "relaxation–oscillations". *Lond. Edinb. Dublin Philosoph. Mag. J. Sci. Ser. 7*, **2**, 978–992 (1926).

[3] Kuramoto, Y. *Chemical Oscillations, Waves, and Turbulence*. Dover (2003).

[4] Suchorsky, M.K., Sah, S.M., Rand, R.H.: Using delay to quench undesirable vibrations. *Nonlinear Dynamics*, **62**, 407–416 (2010).

[5] Atay, F.M.: Van der Pol's oscillator under delayed feedback. *J. Sound Vib.*, **218**(2), 333–339 (1998).

[6] Wirkus, S., and Rand, R.: Dynamics of Two Coupled van der Pol Oscillators with Delay Coupling. *Nonlinear Dynamics*, **30**, 205–221 (2002).

[7] Das, S. L. and Chatterjee, A.: Multiple scales without center manifold reductions for delay differential equations near Hopf bifurcations. *Nonlinear Dynamics*, **30** (4), 323–335 (2002).

[8] Mendelowitz, L., Verdugo, A., and Rand, R.: Dynamics of three coupled limit cycle oscillators with application to artificial intelligence, *Communications in Nonlinear Science and Numerical Simulation*, **14** (1), 270–283 (2009).

[9] Baesens, C., Guckenheimer, J., Kim, S., MacKay, R.S.: Three coupled oscillators: mode–locking, global bifurcations and toroidal chaos, *Physica D*, **49** (3), 387–475 (1991).

[10] Zhang, M., Wiederhecker, G.S., Manipatruni, S., Barnard, A., McEuen, P., and Lipson, M.: Synchronization of Micromechanical Oscillators Using Light, *Physical Review Letters*, **109** (23), 233906 (2012).

[11] Cohen, A.H., Holmes, P.J., and Rand, R.H.: The Nature of the Coupling Between Segmental Oscillators of the Lamprey Spinal Generator for Locomotion: A Mathematical Model, *Journal of Mathematical Biology*, **13** (3), 345-369 (1982).

[12] Keith, W. L. and Rand, R. H. (1984), 1:1 and 2:1 phase entrainment in a system of two coupled limit cycle oscillators, *J. Math. Biology*, **20** (2), 133–152.

[13] Doedel, E., Champneys, A., Fairgrieve, T., Kuznetsov, Y., Sandstede, B., Wang, X. (1998), AUTO 97: Continuation and Bifurcation Software for Ordinary Differential Equations.

[14] Rand, R.H., and Holmes, P.J.: Bifurcation of Periodic Motions in Two Weakly Coupled van der Pol Oscillators. *Int. J. Nonlinear Mechanics*, **15**, 387–399 (1980).

[15] Storti, D.W., and Rand, R.H.: Dynamics of Two Strongly Coupled van der Pol Oscillators. *Int. J. Nonlinear Mechanics*, **17**, 143–152 (1982).

[16] Storti, D.W., and Rand, R.H.: Dynamics of Two Strongly Coupled Relaxation Oscillators. *SIAM J. Applied Math.*, **46**, 56–67 (1986).

[17] Belair, J., and Holmes, P.: On linearly coupled relaxation oscillators. *Quart. Appl. Math.*, **42**, 193–219 (1983).

[18] Chakraborty, T., and Rand, R.H.: The Transition from Phase Locking to Drift in a System of Two Weakly Coupled Van der Pol Oscillators. *International J. Nonlinear Mechanics*, **23**, 369–376 (1988).

[19] Cohen, A.H., Holmes, P.J., and Rand, R.H.: The Nature of the Coupling Between Segmental Oscillators of the Lamprey Spinal Generator for Locomotion: A Mathematical Model. *J. Math. Biology*, **13**, 345–369 (1982).

[20] Rand, R.H., Cohen, A.H., and Holmes, P.J.: Systems of Coupled Oscillators as Models of Central Pattern Generators. In: Cohen, A.H. (ed.) Chapter 9 in *Neural Control of Rhythmic Movements in Vertebrates*, pp. 333–368. John Wiley and Sons (1988).

[21] Strogatz, S.H., and Mirollo, R.E.: Stability of Incoherence in a Population of Coupled Oscillators. *Journal of Statistical Physics*, **63**, 613–635 (1991).

[22] Lazarus, L. and Rand, R.: Dynamics of a System of Two Coupled Oscillators which are Driven by a Third Oscillator. *Journal of Applied Nonlinear Dynamics*, **3**(3), 271–282 (2014).

[23] Yeung, M.K.S., and Strogatz, S.H.: Time Delay in the Kuramoto Model of Coupled Oscillators. *Phys. Rev. Let.*, **82**, 648–651 (1999).

[24] Rand, R.H.: *Lecture Notes in Nonlinear Vibrations*, published online by the Internet–First University Press:
http://ecommons.library.cornell.edu/handle/1813/28989 (2012)

[25] Rand, R.: Differential–delay equations. In: Luo, A.C.J., Sun, J.-Q. (eds.) Chapter 3 in *Complex Systems: Fractionality, Time–delay and Synchronization*, pp. 83–117. Springer, Berlin (2011).

[26] Verdugo, A., Rand, R.: Hopf bifurcation formula for first order differential–delay equations. *Commun. Nonlinear Sci. Numer. Simul.*, **12**, 859–864 (2007).

[27] Engelborghs, K., Luzyanina, T., Roose, D.: Numerical bifurcation analysis of delay differential equations using DDE–BIFTOOL. *ACM Trans. Math. Softw.*, **28**(1) 1–21 (2002).

[28] Engelborghs, K., Luzyanina, T., Samaey, G.: DDE–BIFTOOL v. 2.00: a Matlab package for bifurcation analysis of delay differential equations. Technical Report TW–330, Dept. Comp. Sci., K.U.Leuven, Leuven, Belgium (2001).

[29] Heckman, C.R.: Numerical continuation using DDE–BIFTOOL. Appendix B in *Asymptotic and Numerical Analysis of Delay–Coupled Microbubble Oscillators* (Doctoral Thesis). Cornell University (2012).

[30] Lazarus, L., Davidow, M., Rand, R.: Dynamics of a delay limit cycle oscillator with self–feedback. *Nonlinear Dynamics*, **82** (1): 481–488 (2015).

[31] Stepan, G. *Retarded Dynamical Systems: Stability and Characteristic Functions*. Longman Scientific and Technical, Essex, England (1989).

[32] Haselsteiner, A.F., Gilbert, C., Wang, Z.J.: Tiger beetles pursue prey using a proportional control law with a delay of one half–stride. *J. R. Soc. Interface*, **11** (95), (2014).

[33] Insperger, T. and Stepan, G.: Stability analysis of turning with periodic spindle speed modulation via semidiscretization. *Journal of Vibration and Control* **10** (12), 1835–1855 (2004).

[34] Guckenheimer, J., Holmes, P. *Nonlinear Oscillations, Dynamical Systems, and Bifurcations of Vector Fields*. Springer–Verlag, New York (1983).

[35] Rand, R., Barcilon, A., Morrison, M.: Parametric resonance of Hopf bifurcation. *Nonlinear Dynamics*, **39** (4), 411–421 (2005).

[36] Gambaudo, J.M.: Perturbation of a Hopf bifurcation by an external time-periodic forcing. *J. Differential Equations*, **57**: 172–199 (1985).

[37] Moehlis, J.M.: Perturbation of a Hopf bifurcation by resonant temporal forcing. Appendix E in *Forced Symmetry-Breaking as a Mechanism for Bursting* (Doctoral Thesis). University of California at Berkeley (1993).